

See discussions, stats, and author profiles for this publication at: <https://www.researchgate.net/publication/340909725>

Reconstruction of the Tiber Deltaic stratigraphic successions near Ostia using the PADM chart and tracking of the bedload-derived facies (Rome, Italy)

Article in *Geomorphology* · April 2020

DOI: 10.1016/j.geomorph.2020.107227

CITATIONS

0

READS

29

10 authors, including:



Ferreol Salomon

French National Centre for Scientific Research

65 PUBLICATIONS 406 CITATIONS

[SEE PROFILE](#)



Cécile Vittori

University of Strasbourg

16 PUBLICATIONS 100 CITATIONS

[SEE PROFILE](#)



Brice Noiro

Université Lumière Lyon 2

3 PUBLICATIONS 0 CITATIONS

[SEE PROFILE](#)



Elisa Pleuger

University of Liège

21 PUBLICATIONS 120 CITATIONS

[SEE PROFILE](#)

Some of the authors of this publication are also working on these related projects:



The Mammal faunal assemblages from Late Pleistocene of Apulia Peninsula [View project](#)

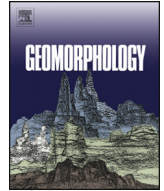


Quaternary of the Upper Rhine Graben [View project](#)



Contents lists available at ScienceDirect

Geomorphology

journal homepage: www.elsevier.com/locate/geomorph

Reconstruction of the Tiber Deltaic stratigraphic successions near Ostia using the PADM chart and tracking of the bedload-derived facies (Rome, Italy)

Ferréol Salomon ^{a,*}, Cécile Vittori ^{a,b}, Brice Noirod ^c, Elisa Pleuger ^{b,d}, Carlo Rosa ^e, Ilaria Mazzini ^f, Pierre Carbonel ^g, Hatem Djerbi ^h, Piero Bellotti ⁱ, Jean-Philippe Goiran ^b

^a French National Center for Scientific Research (CNRS)/Université de Strasbourg, Laboratoire Image Ville Environnement (UMR 7362), 3 rue de l'Argonne, 67083 Strasbourg Cedex, France

^b French National Center for Scientific Research (CNRS), UMR5133-Archéorient, MOM, 7 rue Raulin, 69007 Lyon, France

^c French National Center for Scientific Research (CNRS)/Université de Lyon, Environnement Ville Société (UMR 5600), 18, rue Chevreul, 69362 Lyon Cedex, France

^d Université de Liège, Département de Géologie, UR Argiles, Géochimie et Environnements sédimentaires, Liège, Belgium

^e Istituto Italiano di Paleontologia Umana (ISIPU), Museo Civico di Zoologia, Via Aldrovandi 18, 00197 Rome, Italy

^f CNR- Institute of Environmental Geology and Geoengineering, Area della Ricerca di Roma 1, Via Salaria km 29,300, 00015 Montelibretti, RM, Italy

^g French National Center for Scientific Research (CNRS), UMR 5508-EPOC, 16, rue de Mégret, F-33400 Talence, France

^h Études et valorisation archéologiques Srl (Éveha), 87 avenue des bruyères, 69 150 Décines-Charpieu, France

ⁱ Dipartimento di Scienze della Terra, SAPIENZA Università di Roma, Piazzale A. Moro 5, 00185 Roma, Italy

ARTICLE INFO

Article history:

Received 3 October 2019

Received in revised form 22 April 2020

Accepted 22 April 2020

Available online 24 April 2020

Keywords:

Chronostratigraphy

Palaeoenvironments

PADM chart

Tiber delta

ABSTRACT

Located between the deltaic plain and the subaqueous delta, base level is one of the most important factors that affect depositional elements and the sedimentary architecture of river deltas. In this respect, its changes are essential to reconstruct delta evolution during the Holocene. In this paper, we study three cores drilled in the Tiber delta (Italy). Palaeoenvironmental analyses were performed and included new sedimentological data (laser grain size, loss-on-ignition, magnetic susceptibility), new data from bioindicators (ostracods and macrofauna), and 11 new radiocarbon dates. The three cores were analysed and replaced in a cross section between the Inner and Outer Tiber delta, i.e., in the palaeolagoon and in the progradational delta plain. First, we have mapped the Holocene transgression and progradation of the Ostia area using palaeoenvironmental age-depth modelling techniques (PADMs). PADM charts help to interpret a stratigraphic succession in a river delta. They contribute to the understanding of the links between depositional environments, sedimentation rate, and sea level rise and to reconstruct coastline trajectories. More precisely, they contribute to the interpretation of the consequences of the sea level jumps dated to the 9000–8000 cal. BP period on coastal environments and help to identify progradational phases (around 4 k, and from 2.8 to 2.6 k cal. BP). Second, we identify indirect (fresh-water bioindicators) and direct (bedload-derived facies) evidence of fluvial activity in the studied cross section. The studied deep cores indicate that at least one palaeochannel of the Tiber River was already flowing in the middle/southern part of the delta from 4 k cal. BP. Finally, a first map of the lateral mobility of the palaeochannels of the Tiber River is proposed for the last 6 k cal. BP using the new data and a synthesis of all the data available at the scale of the delta.

© 2020 Elsevier B.V. All rights reserved.

1. Introduction

Geomorphologically, river deltas are composed of a subaerial plain and a subaqueous part separated by the sea level or base level (Wright and Coleman, 1973; Wright, 1977, 1985; Coleman, 1982;

Stanley and Warne, 1994; Hori and Saito, 2007; Anthony et al., 2014). The existence of deltas depends primarily on the sediment load transported by the rivers to the sea and on the coastal and marine conditions. River channels are essential to route sediment to the coastlines and contribute to shape the deltas. In parallel, the sedimentary architecture of river deltas is mainly controlled by the base level that changes over time. It is a key factor that affects the characteristics and the location of fluvial, coastal, and marine facies. The reconstruction of the formation of river deltas during the Holocene depends on an integrated approach, taking into account a large range of data such as sediment facies, facies distribution,

* Corresponding author.

E-mail addresses: ferreol.salomon@live-cnrs.unistra.fr (F. Salomon), elisa.pleuger@uliege.be (E. Pleuger), ilaria.mazzini@igag.cnr.it (I. Mazzini), hatem.djerbi@eveha.fr (H. Djerbi), jean-philippe.goiran@mom.fr (J.-P. Goiran).

unconformities, relative sea level change, and accommodation space. In this regard, methods, notions, concepts, and visualisation tools developed in sequence stratigraphy are essential (Posamentier and James, 1993; Catuneanu, 2006; Catuneanu et al., 2009; Embry et al., 2007). The time-stratigraphic context is also crucial to interpret sediment deposits in sequence stratigraphy. We suggest testing the Palaeoenvironmental-Age Depth Model (PADM chart) to visualise and interpret links between sedimentary facies, the relative sea level change rate, and the sedimentation rate (Salomon et al., 2016a). It corresponds to a classic age-depth model, but instead attempts to integrate a wide range of relevant data to interpret deltaic sediment deposits by using concepts developed in sequence stratigraphy.

In this study, we not only consider coastal and marine sediments and their relation to the Holocene base level, but also consider river deposits even though they follow different trends. It is very easy to spot the current channels, but multiple channels have existed throughout the Holocene that are less easy to identify. The palaeogeographical reconstruction of river mobility in deltas through the Holocene is a challenge. During the Early Holocene transgressive phase, the identification of river mouth palaeochannels is based on sedimentary cores. Their locations are mostly because of chance or a large chronostratigraphic database with many cores, palaeoenvironmental analyses and dates. In this case, palaeogeographical reconstruction of the Holocene transgression of the river mouth area of the Rhine is remarkable (Hijma and Cohen, 2011). The locations of the deltaic river courses or the river mouths are easier for younger stages of delta formation: when base level rise stalls, a high stand is established and the delta system becomes progradational. The progradational phase started around 6500 cal. BP in the Mediterranean area because of the sea level rising more slowly (Nile delta: Stanley and Warne, 1993, 1994; Po delta: Amorosi et al., 2017; Stefani and Vincenzi, 2005; Rhone delta: Vella and Provansal, 2000; Vella et al., 2005; Ebro delta: Sornoza et al., 1998; Cearreta et al., 2016). From these youngest millennia, some morphological changes are noticeable on the ground surface. Palaeochannels, beach ridges, and palaeolagoons can be traceable through aerial photography, satellite imagery, old maps, or LiDAR data. Palaeochannels can be characterised by their morphologies (levees, ridges and swales, cut-off channels) or their location is inferred when they cut pre-existing beach ridges (Pranzini, 2007; Ullmann et al., 2018; Gebremichael et al., 2018). Alternatively, palaeoriver mouths can be located using beach ridges in cuspidate deltas (Stefani and Vincenzi, 2005; Vella et al., 2005) or by producing submarine topographic/geophysical profiles of subaqueous lobe deltas (Shaw et al., 2016). However, through time, floodplain deposits and coastal dynamics, respectively, contribute to cover and rework morphological evidence.

Typically, studies on coastal palaeodynamics are more numerous than studies on fluvial palaeodynamics of the adjacent delta plain inland. This can be attributed to a better record of coastal morphologies on aerial photography/satellite imagery (beach-ridges), and also because coastal dynamics are better expressed vertically in relation to the base level (RSL - Relative Sea Level). Progradational beach ridges can extend widely along the coast and can be studied using perpendicular cross sections (dates of the progradational phases and identification of potential erosional or stability phases) (Bicket et al., 2009 for the Tiber delta). The location of palaeochannels is more difficult to predict (especially when it involves avulsion processes), and river systems often rework older alluvial morphologies. In recent years, this discrepancy between coastal and fluvial studies tends to be filled by an increasing number of sedimentary drillings, as well as the development of LiDAR data. For example, the recurrent discussion about the identification of Nile River branches is currently reexamined by LiDAR data from TamDEM-X (Gebremichael et al., 2018; Ullmann et al., 2018).

This paper focuses on cores drilled between 2011 and 2013 down to 25 m in the area of the archaeological site of Ostia (Figs. 1 and 2). The studied cross section includes the turning point between the last phase of the transgression and the early phases of the progradation (Figs. 2 and 3). Palaeoenvironmental Age-Depth Models (PADM charts) are made to clarify the interpretation of this coastal area and display the effect of river erosion in the stratigraphies.

2. Geological and geomorphological settings

The Tiber delta is located in the Tyrrhenian extensional continental margin. This configuration started during the Miocene and shaped the landscape with northwest/southeast normal faulting and northeast/southwest transverse systems in the lower Tiber (Funicello, 1995). The Tiber delta is developing near Upper-Middle Pleistocene volcanoes on the east of the Tyrrhenian Sea back arc basin (Karner et al., 2001b) and takes part of the Quaternary succession starting in the Late Pliocene near Rome (Milli, 1997; Karner et al., 2001a). General uplift of the area is related to volcanic activity and isostasy (De Rita et al., 1994; Ferranti et al., 2006; Mantovani et al., 2009). Active faults in the Tiber delta during the Holocene are still discussed by different research teams (Bigi et al., 2014; Ciotoli et al., 2016; Marra et al., 2019) (Fig. 1).

The Tiber delta is a wave dominated delta (Bellotti et al., 1994). The Tiber River is 405 km long with a spring at 524 m a.s.l. The watershed area is 17,375 km² (Autorità di Bacino del Fiume Tevere, 2006). Today, the regime of the Tiber River is pluvio-nival with maximum mean discharge in winter (February) and minimum mean discharge in summer (August). During the twentieth to twenty-first centuries the annual water discharge is 213 m³/s, with a minimum at 62 m³/s (August 1986) and a maximum at 2750 m³/s (December 1937) (Bersani and Bencivenga, 2001). The first palaeogeographical reconstructions date to the 1950s and 1960s with the aerial-photo interpretation of J. Bradford (1957 - Fig. 23) and a geological map (Segre in Dragone et al., 1967). In the context of the construction of the International Airport of Rome - Fiumicino, Segre (1986) hypothesized the presence of many palaeochannels in the Tiber delta. The first palaeogeographical reconstruction, based on sedimentary cores and radiocarbon dates, was proposed in the 1980s (Belluomini et al., 1986). Later, reconstructions based on an integrated approach of sedimentary cores, sedimentological analysis, palaeoenvironmental data, and sequential stratigraphy were coordinated by Bellotti (Bellotti et al., 1994, 1995, 1989, 2007, 2018), and more recently by Milli (Amorosi and Milli, 2001; Milli et al., 2013, 2016). These studies contributed in reconstructing the formation of the prodelta, the delta front, and the deltaic plain during the Holocene. Traditionally, the Tiber delta plain is divided into two main geomorphological units; the inner delta plain occupied by the palaeolagoon of Ostia and Maccarese, and the outer delta plain corresponding to the prograded deltaic plain.

Similar to other river deltas across the world, two periods characterise the evolution of the Tiber river mouth since the **Last Glacial Maximum**. Following the quick sea level rise starting around 16,500 cal. BP (Lambeck et al., 2014), transgression affected the Tiber River mouth and contributed to the formation of a specific sedimentary sequence: the Transgressive Systems Tract (TST). Afterwards, since 7000-6000 cal. BP, sea level rise slowed down and the Tiber delta started to form a large prograded plain (Bellotti et al., 2007). During this second period, sedimentary deposits belong to the Highstand Systems Tract (HST). More detailed analysis of the phases of progradation and erosion are proposed by Giraudi (2004) and Bicket et al. (2009). For the last 2000 yr, archaeological and historical data can be used to reconstruct fluvial and coastal mobility (Le Gall, 1953; Bersani and Moretti, 2008) and can be combined with sedimentary cores, ¹⁴C and OSL dates (Salomon, 2013).

Many hypotheses exist for the location of the river channels or channel belts in the Tiber delta during the Holocene (Dragone et al.,

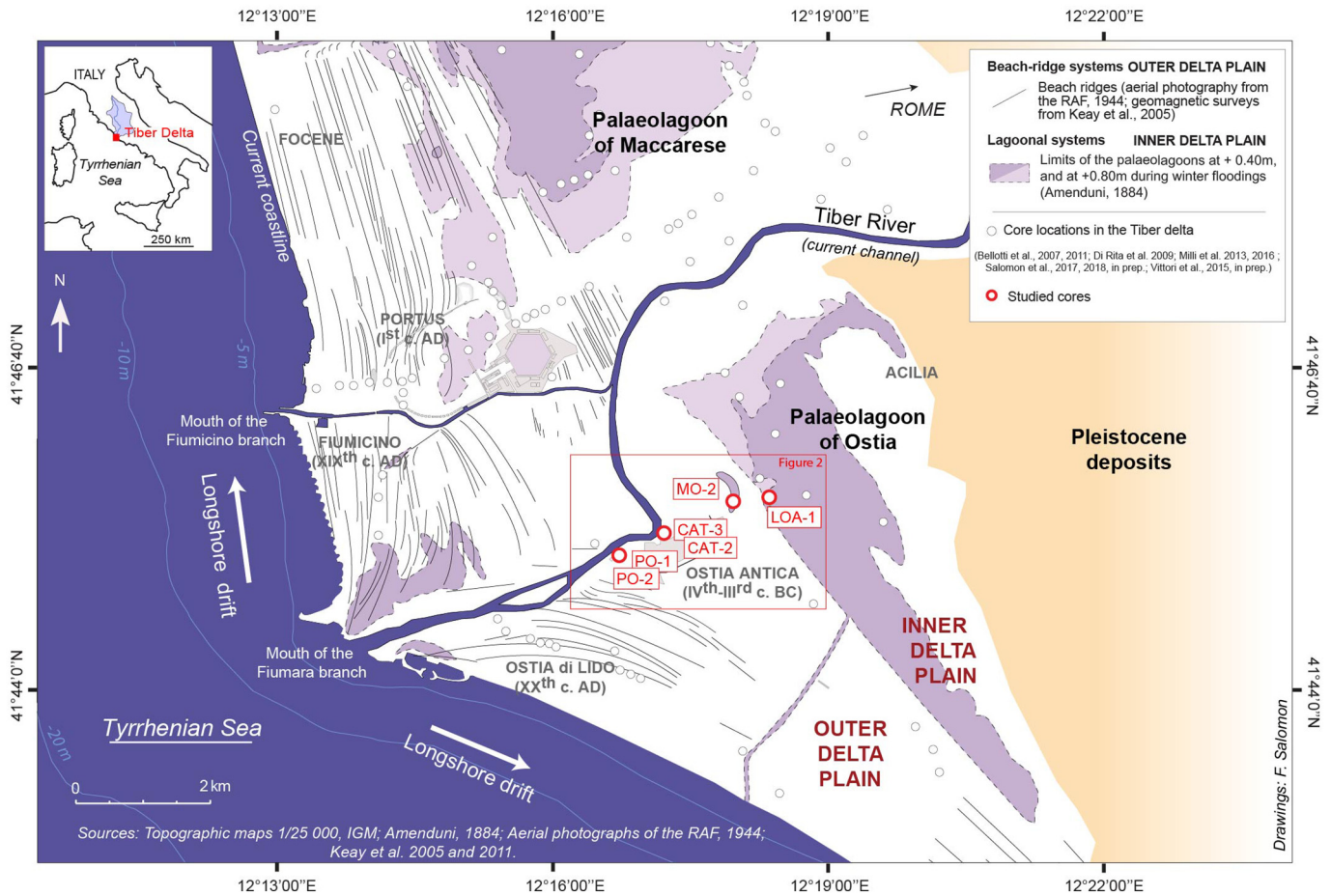


Fig. 1. Study area location. The map exposes the geomorphology of the Tiber delta and core locations. Other factors possibly affected the geomorphology of the Tiber delta like the depth of the unconformity at the base of the Tiber Depositional Sequence available in Milli et al. (2013), or faults hypothesized in Bigi et al. (2014), Ciotoli et al. (2016), Marra et al. (2019). However, there is no consensus yet related to the activity of the faults in the Tiber delta during the Holocene.

1967; Segre, 1986; Bellotti et al., 2007; Giraudi et al., 2009). The topography of the unconformity at the base of the Tiber Depositional Sequence confines the lateral instability of the river channels in the centre of the Tiber delta during the early stages of the transgression (13,000–9000 cal. BP–Bellotti et al., 2007; Milli et al., 2013). Main phases of evolution suggest a channel belt of the Tiber in the central axis of the delta during the Early Holocene (>9000 cal. BP–Bellotti et al., 2007; Milli et al., 2013, 2016), and a displacement of the channel belt towards the south until today (<9000 cal. BP–Bellotti et al., 2007). The identification of palaeochannels visible in aerial photography, satellite imagery, and old maps makes it possible to reconstruct the evolution of the lateral mobility of the Tiber during at least the last 2500 yr (Arnoldus-Huyzendveld and Paroli, 1995; Arnoldus-Huyzendveld and Pellegrino, 1999; Salomon et al., 2017, 2018). The first detailed description of the bedload-derived facies for the Tiber delta is proposed for the bottom of the channels of the meander of Ostia dated between the end of the first millennium BCE and 1557 CE (bedload-derived deposits at the bottom of the point bar and at the bottom of the oxbow –Salomon et al., 2017). Studies based on cores drilled in the coastal area (Goiran et al., 2010; Salomon, 2013; Goiran et al., 2014), in the palaeolagoon of Ostia (Bellotti et al., 2011; Vittori et al., 2015) and in palaeochannels of the Tiber River of Ostia (Salomon et al., 2017, 2018), suggest a migration of the last section of the course of the Tiber in its delta towards the south between 2800 cal. BP and 2300–1700 cal. BP. Most of the evidence is from indirect fluvial influence suggested by bioindicators (Bellotti et al., 2011; Goiran et al., 2014). Recently, coarse bedload-derived facies from this period have been dated

just north of Ostia (Hadler et al., 2020, Core TEV2A/TEV DP8), and could be product of the initial phase of formation of the palaeomeander of Ostia (Salomon et al., 2017, 2018). Earlier phases of the fluvial evolution are still to be tracked and dated with precision.

3. Methods

This paper includes new chrono-stratigraphical and palaeoenvironmental data from Cores PO-1 and 2, CAT-3 and MO-2. The upper parts of these cores were previously published and studied with a geoarchaeological perspective. These upper stratigraphic sequences were interpreted in regards to the evolution of the Roman city of Ostia (Core MO-2 in Salomon et al., 2017; Cores CAT-2 and CAT-3 in Salomon et al., 2018) and its harbours (PO-1 and 2 in Goiran et al., 2014). Core LOA-1 (Vittori et al., 2015), Core CAT-2 (Salomon et al., 2018) and Core OST-4 (Hadler et al., 2015) complement the cross section.

Cores PO-1/PO-2, CAT-2/CAT-3, and MO-2 were drilled between 2010 and 2013. Stratigraphies record a large range of sedimentary facies and were analysed using palaeoenvironmental indicators classically used in such context (Figs. 4, 6, and 8). Before any destructive analysis, the magnetic susceptibility of the core sequences were measured in CGS using a Bartington MS2E1 (Dearing, 1999). In the Tiber delta, the magnetic susceptibility records content of clinopyroxenes and magnetites coming from the volcanic areas of the watershed (Belfiore et al., 1987). High magnetic susceptibility is primarily observed in the sand fraction of the fluvial bedload-derived facies or in coastal sandy placers

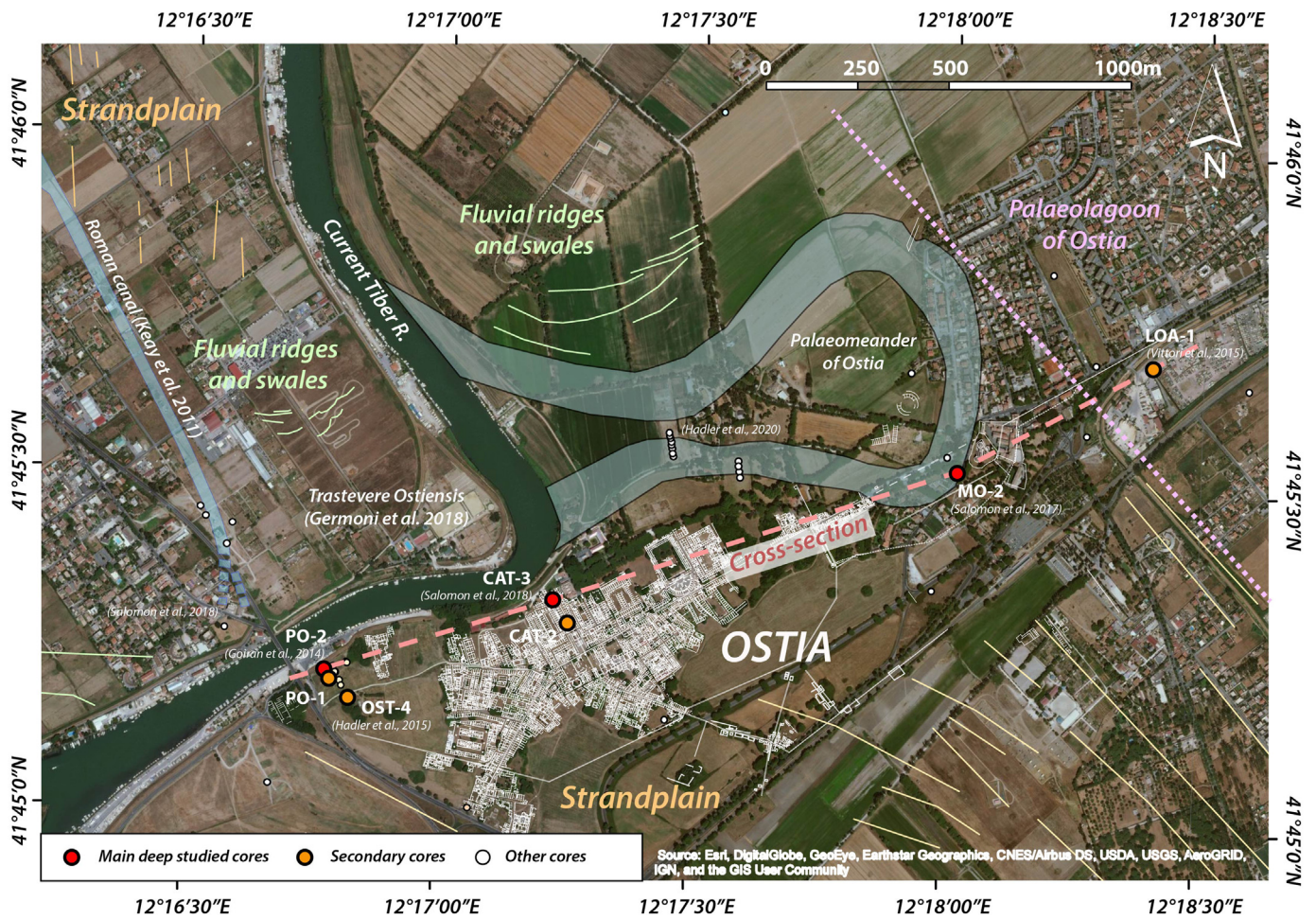


Fig. 2. Location of the studied cores and other boreholes drilled in the area of Ostia. Archaeological remains of Ostia and neighboring structures (white lines) are reported along with the main geo-features identified in this area of the Tiber delta (location of the palaeolagoon of Ostia according to Amenduni, 1884).

formed along the coast. Magnetic susceptibility is mainly used here to support the delineation of stratigraphical units. Palaeohydrodynamic context is deduced from grain-size analyses. Wet sieving at 63 μm and 2 mm was systematically applied to the sediments sampled from the different units of the core stratigraphies. For selected samples distributed in all stratigraphical units, wet sieving was completed with detailed grain size analysis conducted on a laser particle analyzer from Malvern Panalytical. Common grain size indicators such as sorting and median were calculated (Folk and Ward, 1957; Cailleux and Tricart, 1959). Loss-on-Ignition measurements were also conducted on sediments heated at 550 $^{\circ}\text{C}$ for 4 h (for organic matter) and 950 $^{\circ}\text{C}$ for 2 h (for carbonates) following the method proposed by Heiri et al. (2001).

Palaeoecological context is based on the analysis of macrofauna and ostracods. Macrofauna was extracted from sieved samples >2 mm (Perès and Picard, 1964; Bellan-Santini et al., 1994). In the sieved sediments ($63 \mu\text{m} < x < 1 \text{mm}$), all ostracods (small bivalved crustaceans) were picked and normalised to 10 g of sediment weight (Carbonel, 1988; Frenzel and Boomer, 2005; Mazzini et al., 2011; Ruiz et al., 2005; Vittori et al., 2015). Macrofauna and ostracods were identified in order to deduce, in particular, the freshwater and marine influences and the depositional context (Goiran, 2001; Marriner et al., 2006; Goiran et al., 2011). Ostracods from Core PO-2 presented here were also published in Sadori et al. (2016).

Palaeoenvironmental Age-Depth Models (PADM charts) are used to interpret chronometric and integrated stratigraphy data (Salomon et al., 2016a) (Figs. 5, 7 and 9). Developed to interpret ancient coastal harbours and to cross datasets of different types and disciplines, this

PADM chart is related to geohistory diagrams, also called backstrip diagrams (Van Hinte, 1978; Allen and Allen, 2013). The PADM chart is based on a classic age-depth model, with stratigraphical and palaeoenvironmental context recorded on the y-axis, and palaeogeographical and chronological information transferred to the x-axis. The standardised PADM chart integrates all relevant data to interpret the stratigraphical sequences. A quick glance at the charts offers an overview of the local modelled sea level curve, the different apparent sedimentation curves, the results of the palaeoenvironmental analyses and their interpretations. Most importantly, this chart simplifies the identification of sediments related to the Transgressive Systems Tract or the Highstand Systems Tract. Additionally, the systematic combination of the sea level curve with a sedimentation curve exposes clear correlations to their respective evolutions or the variability of the accommodation space through time.

The sedimentation curve is reconstructed with no vertical adjustments –i.e., without any decompaction, subsidence or uplift corrections. The calibration of radiocarbon ages has been performed using the curve proposed by Reimer et al. (2013) with the software OxCal (Ramsey, 1995; Ramsey and Lee, 2013) (Table 1). No model was used to calibrate and narrow down age ranges (e.g., Bayesian model). Interpretative sedimentation curves are proposed based on radiocarbon dates. Between dates the sedimentation curves can be adjusted depending on the processes hypothesized (e.g., sediment starvation, condensed section). Only the *apparent sedimentation curve* and the *apparent accommodation space* are reported here. Interpretations will be proposed consequently. Many papers suggest decompaction methods taking into account the

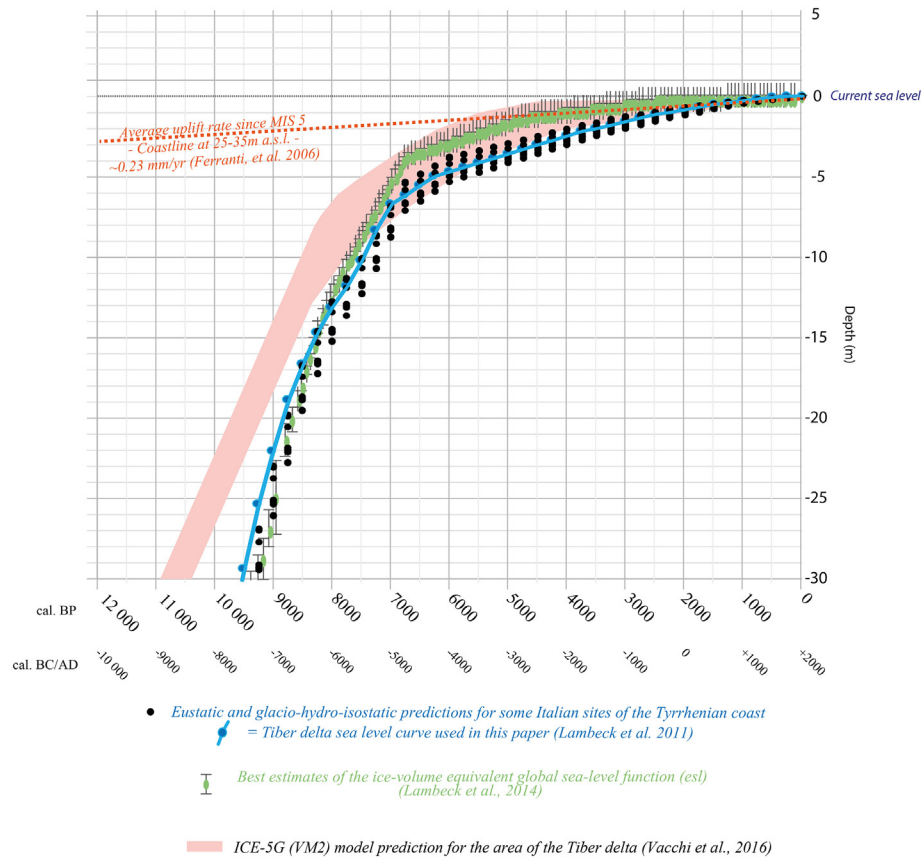


Fig. 3. Reconstructed relative sea level curves and best estimations at local, regional and global scales for the Holocene (Lambeck et al., 2011, 2014; Vacchi et al., 2016). The modelled eustatic and glacio-hydro-isostatic prediction for the Tiber delta will be used (Lambeck et al., 2011).

stratigraphy, porosity, grain size, organic matter content, deposition rate, and overload weight (water or sediment) (Van Hinte, 1978; van Asselen et al., 2009; Kominz et al., 2011; Allen and Allen, 2013; Johnson et al., 2018). A decompaction method was also applied to the Tiber delta (Marra et al., 2013). However, the unconformity at the base of the Tiber Depositional Sequence is not precisely known in the studied area (only estimations are proposed in Milli et al., 2013, between 30 and 40 m below Ostia) and stratigraphies of the Late Pleistocene/Early Holocene are not known for the cores presented here. If the interplay between sedimentation rate, compaction, and tectonics can be discussed, the main phases of the chronology proposed are not affected by this vertical instability. The sea level curve used in this paper is a eustatic curve with glacio-hydro-isostatic predictions proposed by Lambeck et al. (2011) for the Tiber delta. In Fig. 3, this local modelled curve is compared to the best estimate of the ice-volume equivalent global sea level function (Lambeck et al., 2014) and the modelled sea level curve for the Tiber delta area from Vacchi et al. (2016) (ICE-5G VM2 Model). The age-depth models (apparent sedimentation rates) and the palaeoenvironments will be interpreted taking into account their relations to the local sea level curve prediction. The sedimentation curves proposed in this paper are not taking into account the elevation loss caused by sediment compaction (van Asselen et al., 2009; Marra et al., 2013). Possible vertical changes (compaction, neotectonic) will be considered in regards to several parameters: it is suggested that the aspect of the *apparent sedimentation curve* is constrained by the palaeoenvironmental characteristics of the deposits (e.g. subaerial and subaqueous bioindicators, shallow or deep water sediment characteristics), the depositional processes involved, the geometry and the temporal development of the transgressive/progradational sequences (Tamura et al., 2003; Tanabe et al., 2006; Milli et al., 2016), and to a certain extent by the modelled local sea level curve (Lambeck et al., 2011 for the present paper).

4. Analyses

Cores **PO-2**, **CAT-3** and **MO-2** are described in detail (Figs. 4 to 9), and observations in the other cores are used as supporting information. The upper sequences above the bold erosional boundaries lines in Fig. 10 are already published: PO-2 in Goiran et al. (2014) and Sadori et al. (2016) (Harbour of Ostia Sequence); CAT-3 in Salomon et al. (2018) (stratigraphy of a palaeochannel of the Tiber River); and MO-2 in Salomon et al. (2017) (stratigraphy of a palaeochannel of the Tiber River). In Group 1, Core PO-2 will be completed by cores PO-1 (new data for the lower part of the sequence) and Core OST-4 (Hadler et al., 2015). In Group 2, Core CAT-3 will be completed by Core CAT-2. Core MO-2 is the only one forming Group 3, and Core LOA-1 is the only one for Group 4.

Core PO-2 is the deepest reaching core in the Ostia study area (25 m b.s.l.) and the sedimentation refers to a long period of time between 8000 and 2000 cal. BP (Figs. 4 and 5). Four main units were observed below the Roman harbour of Ostia, Units A to D. Unit A is composed of bedded grey silty sand. Around 22 m b.s.l., few cm-layers are composed of silts or organic material. Ostracods mainly reveal a coastal assemblage, mostly brackish lagoonal, but with a large amount of marine and phytal coastal species. No date is available for this unit. Silty sands are still deposited in Sub-unit B1 but interbedded with grey silty clay. In Sub-unit B2, the deposits are compact grey silty clay with no more sandy layers visible (96% of silt and clay). Ostracod assemblage is similar to Unit A. Organic material was radiocarbon dated at 7677 to 7588 cal. BP (6790 ± 30 BP). Silty sand layers are observed again in Unit C (30% of sand). This includes small cm-layers in Unit C1 and sandy deposits in Unit C2 over several decimetres thick. Sub-unit C3 is back to grey silty clay deposits. Interestingly, freshwater ostracods are identified at the bottom of Unit C, but brackish lagoonal deposit assemblages increase in this layer. Organic matter was dated to 4520 to 4296 cal. BP (3955 ± 30 BP) at 14.34 m b.s.l. Bedded grey sand with silty layers

Table 1
Radiocarbon dates - calibrated with the IntCal13 curve -Reimer et al. (2013) (materials in blue and with an asterisk are calibrated with the Marine13 curve -Reimer et al., 2013).

| Core | Sample | Depth below surface (m) | Depth below sea level (s.l.m - Genoa) (m) | Lab. sample | Dating support | ¹⁴ C yr B.P. | ± | Age calibrated BCE-CE (Reimer et al., 2013) - 2σ | Age calibrated cal. BP (Reimer et al., 2013) - 2σ | Reference |
|---|--------------------|-------------------------|---|-------------|----------------|-------------------------|----|--|---|----------------------|
| Area of the palaeolagoon of Ostia | | | | | | | | | | |
| LOA-1 (+0.45m) | LOA-1 / 1308 | 13.08 | -12.63 | Lyon-10104 | Plant material | 175 | 30 | AD 1656 to 1950 | 294 to 0 | Vittori et al., 2015 |
| LOA-1 | LOA-1 / 503 | 5.03 | -4.58 | Lyon-10105 | Shell* | 2660 | 30 | 506 to 336 BCE* | 2456 to 2286 | Vittori et al., 2015 |
| LOA-1 | LOA-1 / 584 | 5.84 | -5.39 | Lyon-10106 | Peat | 2560 | 30 | 805 to 553 BCE | 2755 to 2503 | Vittori et al., 2015 |
| LOA-1 | LOA-1 / 596 | 5.96 | -5.51 | Lyon-10107 | Peat | 2535 | 30 | 798 to 546 BCE | 2748 to 2496 | Vittori et al., 2015 |
| LOA-1 | LOA-1 / 644 | 6.44 | -5.99 | Lyon-10108 | Peat | 2535 | 30 | 798 to 546 BCE | 2748 to 2496 | Vittori et al., 2015 |
| LOA-1 | LOA-1 / 677 | 6.77 | -6.32 | Lyon-10109 | Peat | 2940 | 30 | 1257 to 1044 BCE | 3207 to 2994 | Vittori et al., 2015 |
| LOA-1 | LOA-1 / 747 | 7.47 | -7.02 | Lyon-10110 | Peat | 2835 | 30 | 1107 to 911 BCE | 3057 to 2861 | Vittori et al., 2015 |
| LOA-1 | LOA-1 / 783 | 7.83 | -7.38 | Lyon-10097 | Peat | 3175 | 30 | 1506 to 1402 BCE | 3456 to 3352 | Vittori et al., 2015 |
| LOA-1 | LOA-1 / 823 | 8.23 | -7.78 | Lyon-10098 | Peat | 3240 | 30 | 1611 to 1439 BCE | 3561 to 3389 | Vittori et al., 2015 |
| LOA-1 | LOA-1 / 1595 | 15.95 | -15.5 | Lyon-9323 | Organic matter | 6800 | 30 | 5576 to 5623 BCE | 7526 to 7573 | Vittori et al., 2015 |
| Area of the palaeomeander of Ostia | | | | | | | | | | |
| MO-1 (+1.79m) | MO-1 / 76 | 2.55 | -0.76 | Ly-8040 | Organic matter | Modern | - | Modern | Modern | Salomon et al., 2017 |
| MO-1 | MO-1 / 1143 | 11.43 | -9.64 | Ly-8041 | Bone | 355 | 25 | AD 1454 to 1634 | 496 to 316 | Salomon et al., 2017 |
| MO-2 (+1.7m) | MO-2 / 260 | 2.6 | -0.9 | Ly-8788 | Wood | Modern | - | Modern | Modern | Salomon et al., 2017 |
| MO-2 | MO-2 / 8.88 m | 8.88 | -7.18 | Ly-8780 | Wood | 2035 | 30 | 159 BC to AD 50 | 2109 to 1900 | Salomon et al., 2017 |
| MO-2 | MO-2 / 9.70m | 9.7 | -8 | Ly-8044 | Wood | 2160 | 25 | 356 to 112 BC | 2306 to 2062 | Salomon et al., 2017 |
| MO-2 | MO-2 / 17.70 m | 17.7 | -16 | Lyon-8807 | Shell* | 9370 | 45 | 8390 to 8180 BC | 10340 to 10130 | New date |
| MO-2 | MO-2 / 17.80m | 17.8 | -16.1 | Lyon-8042 | Posidonia* | 7545 | 35 | 6160 to 5975 BC | 8525 to 7925 | New date |
| MO-2 | MO-2 / 17.80m / 2 | 17.8 | -16.1 | Lyon-8043 | Posidonia* | 7600 | 40 | 6205 to 6015 BC | 8155 to 7965 | New date |
| MO-2 | MO-2 / 18.85 m | 18.85 | -17.15 | Lyon-8790 | Wood | 7655 | 40 | 6590 to 6440 BC | 8540 to 8390 | New date |
| MO-2 | MO-2 / 19.95 m | 19.95 | -18.25 | Lyon-8789 | Wood | 8070 | 40 | 7175 to 6830 BC | 9125 to 8780 | New date |
| MO-2 | MO-2 / 20.70 m | 20.7 | -19 | Lyon-8808 | Shell* | 7965 | 40 | 6575 to 6395 BC | 8525 to 8345 | New date |
| MO-3 (+2m) | MO-3 / 3.35 m | 3.35 | -1.35 | Ly-8781 | Wood | 780 | 30 | AD 1210 to 1281 | 740 to 669 | Salomon et al., 2017 |
| MO-3 | MO-3 / 6 to 6.05 m | 6.025 | -4.025 | Ly-8793 | Charcoal | 2120 | 30 | 344 to 51 BC | 2294 to 2001 | Salomon et al., 2017 |
| MO-3 | MO-3 / 10 m | 10 | -8 | Ly-8792 | Bone | 2230 | 30 | 384 to 204 BC | 2334 to 2154 | Salomon et al., 2017 |
| MO-3 | MO-3 / 14.25 m | 14.25 | -12.25 | Ly-8799 | Shell* | 10070 | 50 | 9250 to 8951 BC* | 11200 to 10901 | Salomon et al., 2017 |

are deposited in Unit D with higher value for magnetic susceptibility. Magnetic susceptibility values rise slowly from 5 to 10 CGS to $10-20 \times 10^{-6}$ CGS but never reached 100×10^{-6} CGS in Units A to C (mean value = 7 CGS). Values rise in Unit D and reach $>1000 \times 10^{-6}$ CGS in Sub-unit D2. Carbonate content is generally rising (up to 30% in Sub-unit D2) while organic matter content decreases in the sedimentary sequence. Additionally, freshwater species are more represented in the ostracods identified in Sub-Unit D1 than in the lower units. Unit D2 contains more *Posidonia*, and some fibers were dated to 2786 to 2686 cal. BP (2955 ± 25 BP). The harbour of Ostia is composed of compact dark grey silts mainly with freshwater ostracods. The harbour is finally sealed

by coarse fluvial deposits (Unit E) and fine fluvial deposits (Unit F) (see Goiran et al., 2014 for a detailed description).

Four layers were identified in Core PO-1 below the Roman harbour sequence (Fig. 10), but the core only reaches 18 m b.s.l. Grey silty clay of Core PO-1/Unit A and Unit C are most probably similar to deposits of Sub-unit B2 and C3 in Core PO-2. Surprisingly, dark coarse sand and small gravels were drilled between 15 and 17 m b.s.l. in Core PO-1. Organic matter in the layer was dated to 2715 to 2363 cal. BP (2455 ± 30 BP), but it is covered by grey silty clay in Unit C, which was dated to 4151 to 3981 cal. BP (3720 ± 30 BP) on a piece of wood laying at -14.64 m b.s.l. PO-1/Unit D corresponds to laminated grey sand similar

| Area of the Castrum in Ostia | | | | | | | | | | |
|------------------------------------|------------------|-------|---------|------------------------|-----------------------|--------------------------|----|------------------|--------------|----------------------|
| CAT-1 (+3.82m) | OST-1 / 632 | 6.32 | -2.5 | Lyon-11777(SacA 40124) | Organic matter | 3325 | 30 | 1687 to 1527 BC | 3637 to 3477 | Salomon et al., 2018 |
| CAT-2 (+4.34m) | OST-2 / 1150 | 11.50 | -7.16 | Lyon-11781(SacA 40128) | <i>Posidonia*</i> | 3365 | 30 | 1383 to 1185 BC* | 3333 to 3135 | Salomon et al., 2018 |
| CAT-2 | OST-2 / 1150 | 11.50 | -7.16 | Lyon-11195(SacA 37181) | Wood | 6805 <i>Rejected</i> | 30 | 5738 to 5638 BC | 7688 to 7588 | Salomon et al., 2018 |
| CAT-2 | OST-2 / 635 | 6.35 | -2.01 | Lyon-11197(SacA 37183) | Organic matter | 3220 <i>Rejected</i> | 30 | 1605 to 1425 BC | 3555 to 3375 | Salomon et al., 2018 |
| CAT-2 | OST-2 / 1124 | 11.24 | -6.9 | Lyon-11780(SacA 40127) | Organic matter | 3720 | 30 | 2201 to 2031 BC | 4151 to 3981 | Salomon et al., 2018 |
| CAT-2 | OST-2 / 885 | 8.85 | -4.51 | Lyon-11196 (SacA37182) | Organic matter | 2500 | 30 | 738 to 537 BC | 2688 to 2487 | Salomon et al., 2018 |
| CAT-2 | OST-2 / 613 | 6.13 | -1.79 | Lyon-11779 (SacA40126) | Wood | 2530 | 30 | 797 to 543 BC | 2747 to 2493 | Salomon et al., 2018 |
| CAT-3 (+4.48m) | OST-3 / 748 | 7.48 | -3 | Lyon-11778(SacA 40125) | Charcoal | 2170 | 30 | 360 to 116 BC | 2310 to 2066 | Salomon et al., 2018 |
| CAT-3 | OST-3 / 780 | 7.8 | -3.32 | Lyon-11782 (SacA40129) | Wood | 2190 | 30 | 361 to 178 BC | 2311 to 2128 | Salomon et al., 2018 |
| CAT-3 | OST-3 / 830 | 8.30 | -3.82 | Ly-16569 | Wood | 2445 | 35 | 755 to 409 BC | 2705 to 2359 | Salomon et al., 2018 |
| CAT-3 | OST-3 / 960 | 9.6 | -5.12 | Lyon-11783 (SacA40130) | Charcoal | 2205 | 30 | 370 to 196 BC | 2320 to 2146 | Salomon et al., 2018 |
| CAT-3 | OST-3 / 1110 | 11.10 | -6.62 | Lyon-11198 (SacA37184) | Charcoal | 3400 | 30 | 1767 to 1623 BC | 3717 to 3573 | Salomon et al., 2018 |
| CAT-3 | OST-3 / 1906 | 19.06 | -14.58 | Lyon-13721 (SacA48504) | Org. matter | 5945 | 30 | 4908 to 4727 BC | 6858 to 6677 | <i>New date</i> |
| Area of the Roman harbour of Ostia | | | | | | | | | | |
| PO-2 (+2.40m) | NA | 3.78 | -1.38 | Ly-8059 (GrA) | Wood | 2040 | 25 | 160 BC to AD 25 | 2110 to 1925 | Goiran et al., 2014 |
| PO-2 | NA | 4 | -1.6 | Ly-8060 (GrA) | Wood | 2040 | 25 | 160 BC to AD 25 | 2110 to 1925 | Goiran et al., 2014 |
| PO-2 | NA | 4.9 | -2.5 | Ly-8061 (GrA) | Charcoal | 1990 | 25 | 44BC to 63AD | 1994 to 1887 | Goiran et al., 2014 |
| PO-2 | NA | 4.9 | -2.5 | Ly-8062 (GrA) | Organic matter | 2050 | 25 | 164 BC to 16 AD | 2114 to 1934 | Goiran et al., 2014 |
| PO-2 | NA | 5.26 | -2.86 | Ly-8063 (GrA) | Plant material | 2025 | 25 | 98 BC to AD 52 | 2048 to 1898 | Goiran et al., 2014 |
| PO-2 | NA | 5.26 | -2.86 | Ly-8064 (GrA) | Wood | 2050 | 25 | 164 BC to AD 16 | 2114 to 1934 | Goiran et al., 2014 |
| PO-2 | NA | 6.045 | -3.645 | Ly-9096 (GrA) | Wood | 2160 | 30 | 358 to 108 BC | 2308 to 2058 | Goiran et al., 2014 |
| PO-2 | NA | 7.035 | -4.635 | Ly-9095 (GrA) | Charcoal | 2185 | 30 | 361 to 172 BC | 2311 to 2122 | Goiran et al., 2014 |
| PO-2 | NA | 8.15 | -5.75 | Ly-9094 (GrA) | Charcoal | 2350 | 40 | 729 to 361 BC | 2679 to 2311 | Goiran et al., 2014 |
| PO-2 | NA | 8.53 | -6.13 | Ly-9093 (GrA) | Charcoal | 2125 | 30 | 348 to 52 BC | 2298 to 2002 | Goiran et al., 2014 |
| PO-2 | NA | 8.705 | -6.305 | Ly-9092 (GrA) | Wood | 2165 | 30 | 359 to 112 BC | 2309 to 2062 | Goiran et al., 2014 |
| PO-2 | NA | 10.5 | -8.1 | Ly-8066 (GrA) | <i>Posidonia*</i> | 2955 | 25 | 836 to 736 BC | 2786 to 2686 | Goiran et al., 2014 |
| PO-2 | PO-2 / 1668-1679 | 16.74 | -14.335 | Lyon-13728(SacA 48511) | Org. matter | 3955 | 30 | 2570 to 2346 BC | 4520 to 4296 | <i>New date</i> |
| PO-2 | PO-2 / 2141-2144 | 21.43 | -19.025 | Lyon-13729(SacA 48512) | Org. matter | 6790 | 30 | 5727 to 5638 BC | 7677 to 7588 | <i>New date</i> |
| PO-1 (+2.36m) | NA | 5.3 | -2.94 | Ly-8045 (GrA) | Wood | 2295 | 30 | 406 to 231 BC | 2356 to 2181 | Goiran et al., 2014 |
| PO-1 | NA | 5.73 | -3.37 | Ly-8046 (GrA) | Wood | 2055 | 25 | 165 BC to AD 4 | 2115 to 1946 | Goiran et al., 2014 |
| PO-1 | NA | 10.85 | -8.49 | Ly-8047 (GrA) | Plant material | 2670 | 30 | 895 to 798 BC | 2845 to 2748 | Goiran et al., 2014 |
| PO-1 | PO-1 / 1680-1720 | 17.00 | -14.64 | Lyon-13722(SacA 48505) | Wood | 3720 | 30 | 2201 to 2031 BC | 4151 to 3981 | <i>New date</i> |
| PO-1 | PO-1 / 1850 | 18.50 | -16.14 | Lyon-13723(SacA 48506) | Org. matter | 2455 <i>Rejected?</i> | 30 | 756 to 413 BC | 2715 to 2363 | <i>New date</i> |
| OST-4 (+4.38m) | OST 4/14 HK | 5.72 | -1.34 | MAMS-19753 | Charcoal | 2229 | 17 | 376 to 207 BC | 2326 to 2157 | Hadler et al., 2015 |
| OST-4 | OST 4/19 + PR | 6.68 | -2.30 | MAMS-19754 | Unident. plant remain | 2562 | 19 | 802 to 597 BC | 2752 to 2547 | Hadler et al., 2015 |

Core PO-2 - Analysis

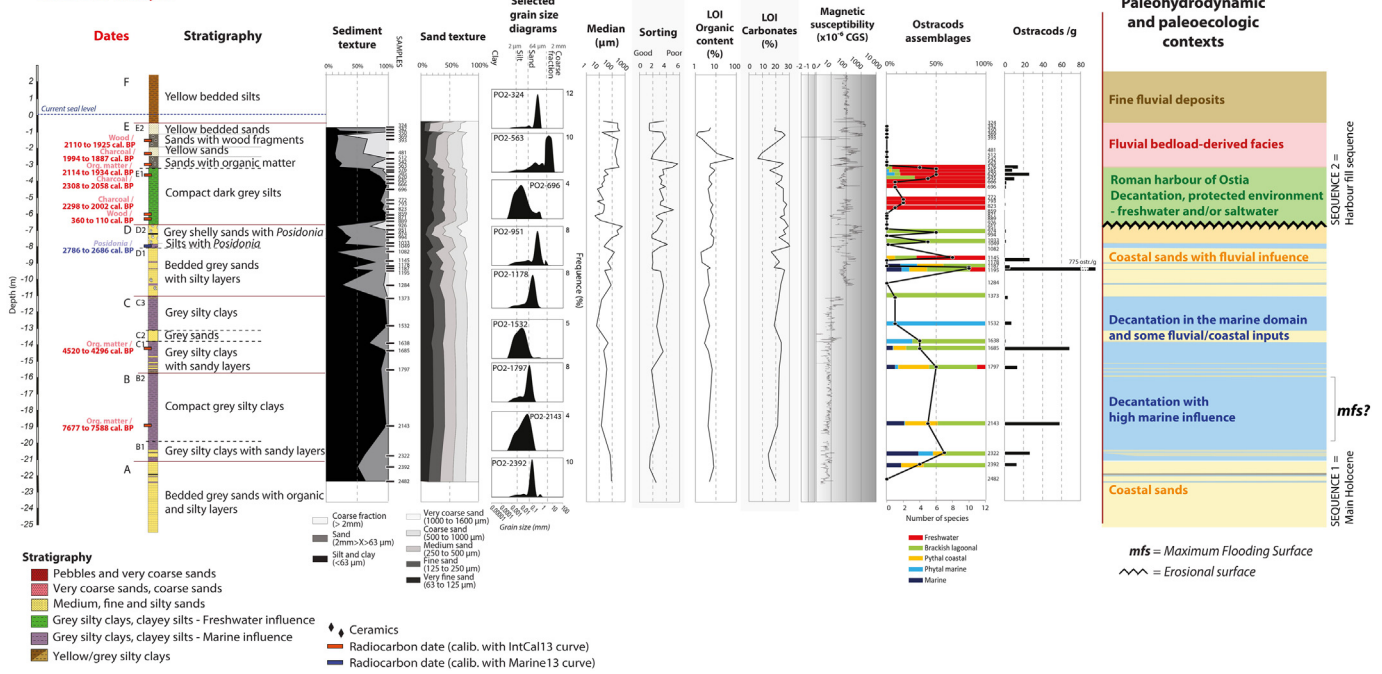


Fig. 4. Sedimentological and palaeoenvironmental analyses of Core PO-2.

to Core PO-1/Unit D. A similar period was obtained for these two layers with a radiocarbon date on plant material at 8.49 m b.s.l. in Core PO-1/UnitD (2845 to 2748 cal. BP, 2670 ± 30 BP). A similar harbour sequence was obtained in Cores PO-1 and 2.

Core OST-4 (Hadler et al., 2015) reveals the upper part of the natural sedimentary sequence that was truncated by harbour excavation during the Roman Republic period, between 2400 and 2100 cal. BP (Units E in cores PO-1 and 2) (Fig. 10). Medium sands are still observed in Unit A and still dated between 2800 and 2500 cal. BP at 2.30 m b.s.l. (2752 to 2547 cal. BP/2562 ± 19 BP). Unit B is a fine deposit of grey silt dated to 2326 to 2157 cal. BP (2229 ± 17 BP) and covered again by sand in Unit C.

Core CAT-3 reaches 16 m b.s.l. (Figs. 6 and 7). Laminated silty fine sands are drilled at the bottom in Unit A. Almost 1 m of grey silt is deposited in Unit B, with low magnetic susceptibility ($<10 \times 10^{-6}$ CGS). Some ostracods were observed in this unit and are associated with brackish environments (*Cyprideis torosa*) or environments without freshwater (*Palmoconcha turbida*, *Leptocythere* sp., *Costa batei*). Charcoals trapped in this protected environment are dated to 6858 to 6677 cal. BP (5985 ± 30 BP). From 13.5 to 6.5 m b.s.l., Unit C is composed of laminated silty sand and the upper part is dated to 3717 to 3573 cal. BP (3400 ± 30 BP). Magnetic susceptibility rises slowly from the bottom to the top of this unit. Sands are mainly fine. Comparatively, these laminated sands are more sorted and finer than in Core PO-2. Ostracods were identified at the bottom of these units and indicate a coastal environment with freshwater influence (*Palmoconcha turbida*, *Costa batei*, *Pontocythere turbida*). An important change in the grain size occurs at 6.51 m b.s.l. Unit D is 1 m thick and composed of 15% to 40% of coarse material. This unit is then covered by almost 3 m of silts (Unit E). Heterometric anthropic material constitutes the upper unit F.

The core sequence of CAT-2 is only reaching 8 m b.s.l. (Salomon et al., 2018), but reveals the upper sedimentation eroded by fluvial mobility between 2800 and 2200 cal. BP in Core CAT-3. Units B and C in CAT-2 are finer deposits in between medium sand in Units A, C and E. Four radiocarbon dates are distributed from the bottom to the top of this stratigraphic sequence. In Core CAT-2/UnitB two radiocarbon dates (4151 to 3981 cal. BP-3720 ± 30 on organic matter - and 3333 to 3135 cal.

BP-3365 ± 30 BP on *Posidonia*) include the time span of the last date obtained in the upper part of Core CAT-3/UnitC (3717 to 3573 cal. BP).

Finally, between 21.30 and 12 m b.s.l., Core MO-2 reveals Early Holocene deltaic deposits settled before the development of the palaeomeander of Ostia between 2400 and 1700 cal. BP (Figs. 8 and 9). The upper 12 m are described in detail in Salomon et al. (2017). The oldest radiocarbon dates of the area are recorded in Unit B and C and covered the period between 8500 and 7900 cal. BP. Unit A (21.30–19.39 m b.s.l.) is mainly composed of silt and clay (56%) with high content of sand (43%). The organic content is only 3% (loss-on-ignition). The macrofauna is particularly interesting. Shells of *Zonites nitidus* were observed, which usually live along shores of lakes and riverbanks. *Oxchilidae* sp. were also identified, which live in terrestrial contexts in wet environments, generally near lakes. Other terrestrial species were observed like *Mediterranea depressa* or other gastropods. No ostracods were identified. The magnetic susceptibility is low, around 10×10^{-6} CGS on average. However, magnetic susceptibility rises in Unit B correlatively with the grain size. Unit B is composed of very well sorted sand with very low organic matter content (1%). A lot of macrofauna fragments were collected including many bivalves sp., gastropods, and other shells difficult to identify. The shells identified are mainly characteristic of sandy or rocky environments (*Bittium reticulatum*, *Cerastoderma edule*, *Rissoa venusta* etc.). *Lentidium mediterraneum* suggests a sandy/clayey bottom close to a river. A marine shell was dated at 8525–8345 cal. BP at 19 m b.s.l. (7965 ± 40 BP). Ostracods identified include *Cyprideis torosa* and *Loxoconcha elliptica*, revealing a brackish environment with high salinity variability, *Loxoconcha rhomboidea*, *Xestoleberis nitida*, *Leptocythere* sp. and *Propontocypris* cf. *prifera*, characterising lagoonal-coastal environments (euhaline) with low salinity changes (polyhaline), and *Cushmanidea* (or *Pontocythere*) *elongata*, *Urocythereis* possibly *favosa*, and *Heterocythereis albomaculata*, typical of a dynamic coastal environment, but with ostracods sometimes hiding in *Posidonia*. Similar to Unit A, deposition in a calm environment is again observed in Unit C, with 95% of silts and clay. Specific diversity reduces in this unit and only some species of *Rissoa linoelata* and *Bittium reticulatum* living in algae, *Posidonia*, or rocks were observed. Some *Posidonia* fibers

Core PO-2 Stratigraphy Palaeoenvironmental Age-Depth Model

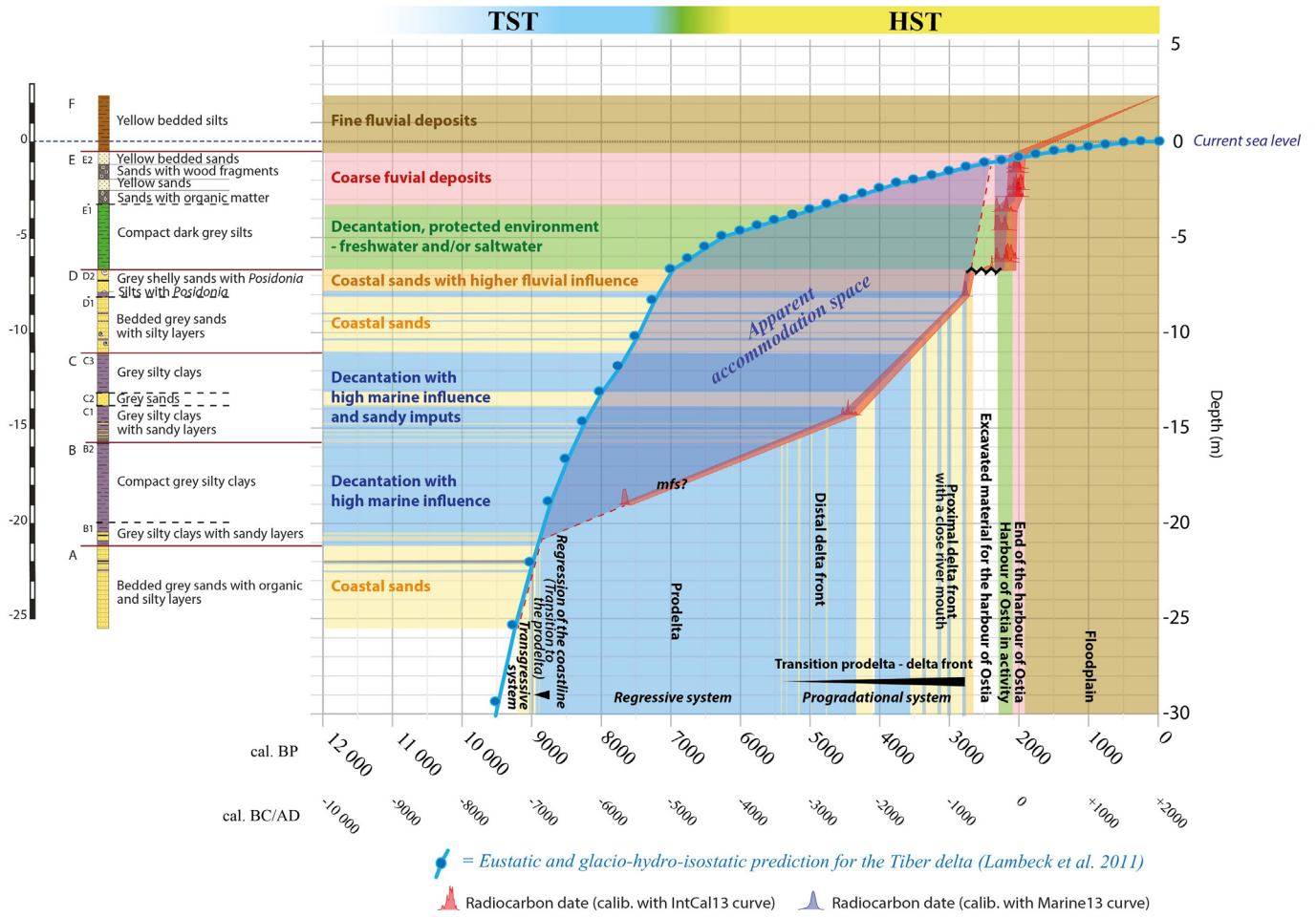


Fig. 5. PADM chart of Core PO-2.

were observed at the top of this unit, which confirms marine influence in this unit. Ostracods reveal a brackish environment, indicating some contact with the sea, but not directly open to the sea (*Loxococoncha rhomboidea*, *Xestoleberis* sp., to infralittoral often with algae, *Cytheridea*, *Paracytheridea*, *Carinocythereis carinata*). Several dates were performed on this unit, from the bottom to the top. At 18.25 m b.s.l. a piece wood was dated to 8070 ± 40 BP and calibrated at 9125–8780 cal. BP. This date is followed at 17.15 m b.s.l. by a date on wood calibrated at 8540–8390 cal. BP (7655 ± 30 BP). In the upper part of this unit, *Posidonia* fibers are dated to 8525–7925 cal. BP (7545 ± 35 BP) and 8155–7965 cal. BP (7600 ± 40 BP). Lastly, laminated silty sands are deposited in Unit D. A sand content of 94% was measured at the bottom but with an average of 76% for all the samples analysed in this unit. Macrofauna exposes species from different environments, from a sandy bottom (*Cerastoderma edule*, *Macra* sp., *Neverita Josephina* ...), or an area near the river mouth (*Zonites nitidus*). Ostracods reveal lagoonal-brackish (*Cyprideis torosa*) to marine environments (*Aurila woodwardii*) with coastal species (*Cushmanidea elongata* and *Urocythereis favosa*). The bottom of Unit D reveals many shell fragments. Most of the shell fragments cannot be identified. A fragment of shell was dated in this unit but should be rejected for the interpretation (9370 ± 45 BP at 16 m b.s. l. – 10,340–10,130 cal. BP). In Unit E, very coarse pebbles were recorded at the bottom with black coarse to very coarse sand. These deposits are the coarsest ever recorded in a Middle/Late Holocene channel of the Tiber in the delta (coarsest pebbles are 2.5 cm (A-axis) × 2 cm (B-axis) × 1 cm (C-axis)). Unit F is an intercalation of

sand and grey silty clay deposited in the Roman period. Finally, unit G is sub-modern deposits of grey silty clay.

5. Discussion

5.1. Interpretation of the depositional contexts and the stratigraphic successions

The study area considered in this paper straddles the inner and the outer delta plain. It crosses part of the palaeolagoon and the area of the archaeological site of Ostia (Fig.2). Fig.10 presents a synthetic cross section interpreting the depositional elements of the studied cores. Core LOA-1 studied in Vittori et al. (2015) is located in the inner deltaic plain and all other studied cores are located in the outer deltaic plain. Sandy deposits identified at the bottom of Cores PO-2 (Unit A) and MO-2 (Unit B) and Unit B in Core LOA-1 are issued from a transgressive sandy coast. Several ¹⁴C and OSL dates confirm that Unit A/Core LOA-1 goes back from the Pleistocene (Vittori et al. in prep.). Units D in Cores PO-1 and PO-2, Unit C in Core CAT-3, Units A, B, C, D, E in Core CAT-2, and Unit D in Core MO-2 are shallowing upward successions related to the progradational delta front. Fine marine sediments deposited in the prodelta are observed in Core PO-1/Units A and C, Core PO-1/Units B and C, Core CAT-3/Unit B, and Core MO-2/Unit C.

Transitions between these three depositional contexts can also be observed. The location of Core PO-2 is the most seaward and the core better records changes in its stratigraphy. The fine interstratification

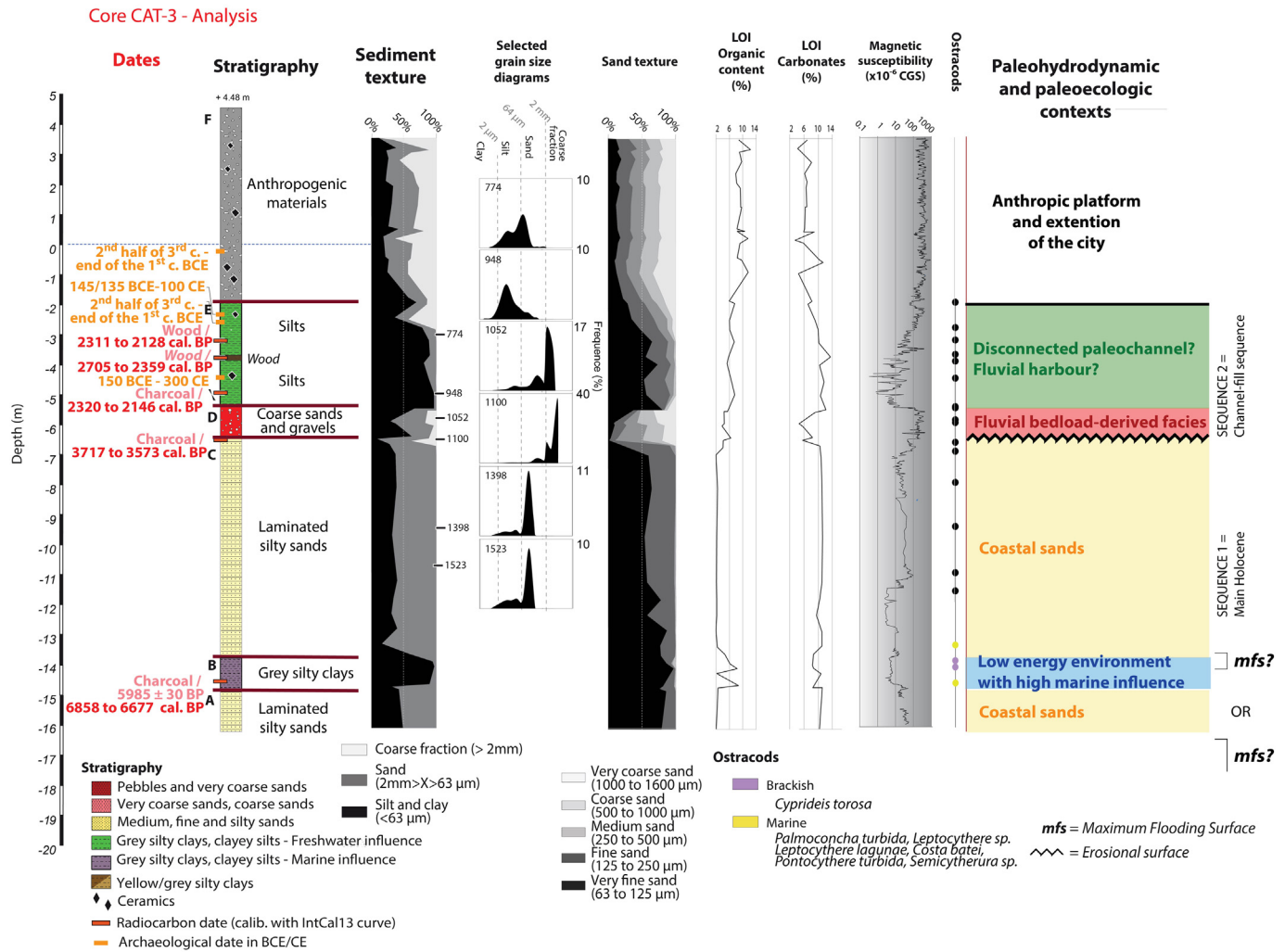


Fig. 6. Sedimentological and palaeoenvironmental analyses of Core CAT-3.

of sand and silty clay in Sub-unit B1 demonstrates change from the transgressive sandy coast (Unit A) to the prodelta (Sub-unit B2). It demonstrates a normal regression of the coastline during the TST. The sandy layers within the grey silty clay in Core PO-2/UnitC correspond to the transition between the prodelta to the delta front. It is the distal delta front part of the progradational system during the HST.

Based on our data, the switch from TST to HST, called the maximum flooding surface (mfs), is not always easy to locate precisely. According to the chronostratigraphy, it seems to happen in the Prodelta in Core PO-2 (Sub-unit B2 - Fig. 4). More analyses would be necessary to identify a slower rate of deposition and a condensed layer of fauna (condensed section). In Core CAT-3, the mfs could be on top of Unit B or not reached by the core. A deeper core, bioindicators, and additional dates would have helped to define it better (e.g., condensed section, sediment starvation, hiatus). The abrupt deepening facies in Core MO-2/UnitC (marine grey silty clay) is covered by a small layer characterised by sediment starvation. It is expressed by high macrofaunal density (hiatus) and can be associated to the mfs (Fig. 8). Finally, the mfs in Core LOA-1 is probably at the limit between Unit B and C.

Late Holocene lateral fluvial mobility removed part of the delta front deposits of the HST in Cores MO-2 (Sequence 2 - Palaeochannel - Units E, F, G) and CAT-1 (Sequence 2 - Palaeochannel/Harbour - Units D and E). In addition, the excavation of the harbour of Ostia during the Roman period also removed progradational sands of the HST in Group 1 area (2400-2000 cal. BP in PO-1 and PO-2 Units E).

In the interpreted cross section between groups 1 and 4, there is currently no clear evidence of fault activity. Deeper cores and complementary dates in the stratigraphies would be necessary to interpret the sequences to examine this further.

5.2. From the TST to the HST: use of the interpretative PADM chart for single core interpretations

According to the PADM charts of Cores PO-2 (Fig. 5), Core CAT-3 (Fig. 7) and Core MO-2 (Fig. 9), the stratigraphies overlap the end of the Transgressive phase and the Progradational phases until 2500 cal. BP.

Amongst the analysed cores, the transgressive coastal sand is only dated in Core MO-2. The sedimentation rate in Units B and C seems to roughly follow the rate of the modelled local sea level curve between 9000 and 8000 cal. BP, which would confirm the validity of the modelled curve of Lambeck et al. (2011). It should be noticed that these four dates at the bottom of Core MO-2 dates sediments from periods often lacking in deltaic sequences or displaying a change of the facies (River deltas worldwide: Stanley and Warne, 1994; Po delta: Amorosi et al., 2017 and Bruno et al., 2017; Rhine delta: Hijma and Cohen, 2011, 2019; Asian deltas: Hori and Saito, 2007; Mississippi delta: Yu et al., 2012). The period 9000-8500 cal. BP is characterised by facies changes related to a sea level jump in Asian deltas (Hori and Saito, 2007). This change is characterised by a shift from coastal/estuarine sand or mud to prodelta mud. A sea level jump would also occur

Core CAT-3

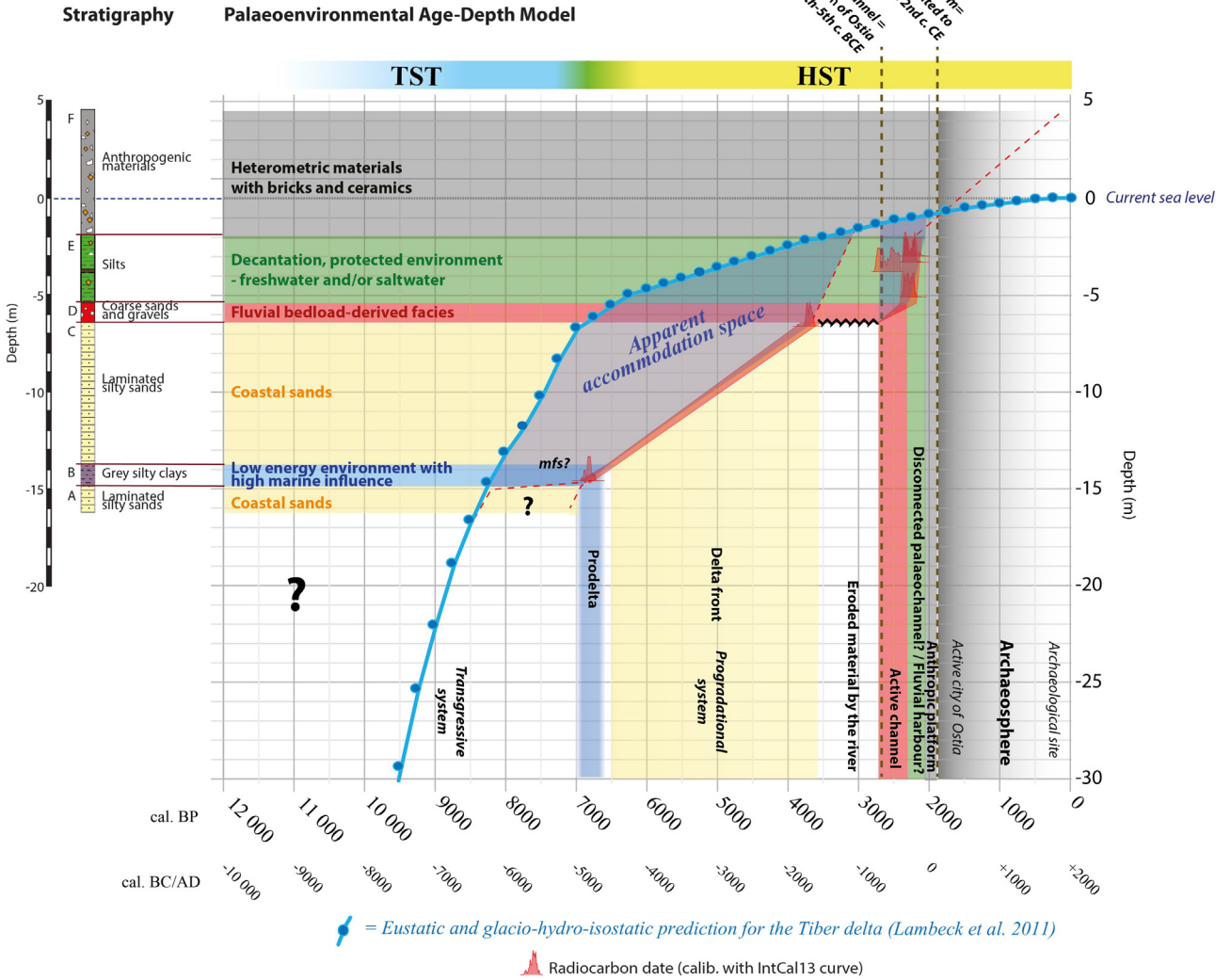


Fig. 7. PADM chart of Core CAT-3.

later between 8500 and 8200 cal. BP, possibly in two phases according to the data from the Rhine delta (Hijma and Cohen, 2019). The marine silty clay from MO-2/UnitC could be related to a rapid deepening facies similar to the observations made by Hori and Saito (2007) for Asian deltas. The modelled curve of Lambeck et al. (2011) for the Tiber delta is correct, but too smoothed to show these sea level jumps. Core MO-2/UnitC offers sedimentation for the period between 9000 and 8000 cal. BP. To support such a sediment rate in a deeper context, the sediment load transported by the Tiber River was probably very important. This strong sedimentation (sandy and fine) could be linked to the Sapropel S1 deposits in the Tyrrhenian Sea (9500–6600 cal BP in Ermeis et al., 2000; 8900–7300 cal. BP in Zanchetta et al., 2007; 10,800–6100 cal BP in De Lange et al., 2008). On top of Unit C, sediment starvation occurs with a hiatus (mfs). The sedimentation rate probably stopped to be consistent with the relative sea level rise, but the chronology is lacking.

At the beginning this sea level jump period, Core MO-2 shows very quickly changing environments from freshwater and terrestrial context in Unit A to a protected environment with high marine influence in Unit C, intercalated with two units of coastal sand in Units B and D. Terrestrial, freshwater, coastal and marine palaeoenvironments seem to be

very close, suggesting a high mobility of the coastline and closely controlled by the rising sea level. Unit A can be associated to a coastal lake or an estuarine environment.

The upper part of Core MO-2 shows a channel-fill sequence (Sequence 2) related to the activity (2400 cal. BP and 1557 CE) and the infill of the palaeomeander of Ostia (1557 CE to the reclamation in the Late nineteenth/Early twentieth century CE-Salomon et al., 2017). Cores S6 and S1 in Bellotti et al. (2011) and Cores E,D and A farther south in Bellotti et al. (2007) demonstrate that sandy deposits continued to be deposited in the upper sequence of Core MO-2 before their removal by the palaeomeander.

The grey silty clay deposits of Core CAT-3/UnitB are dated from 6858 to 6677 cal. BP. Unit B could be just before or contemporary with the transition from the TST to the HST (mfs). A deeper core and complementary analyses would be necessary to identify the mfs. In Fig. 7, two hypothetical sedimentation rates are proposed between Unit A and B. Unit A is either related to the transgressive coast or an instability of the delta front during the TST-HST transition. Unit B is possibly a condensed prodelta layer with a low sedimentation rate (mfs facies similar to Unit B2 in Core PO-2).

Core MO-2 - Analysis

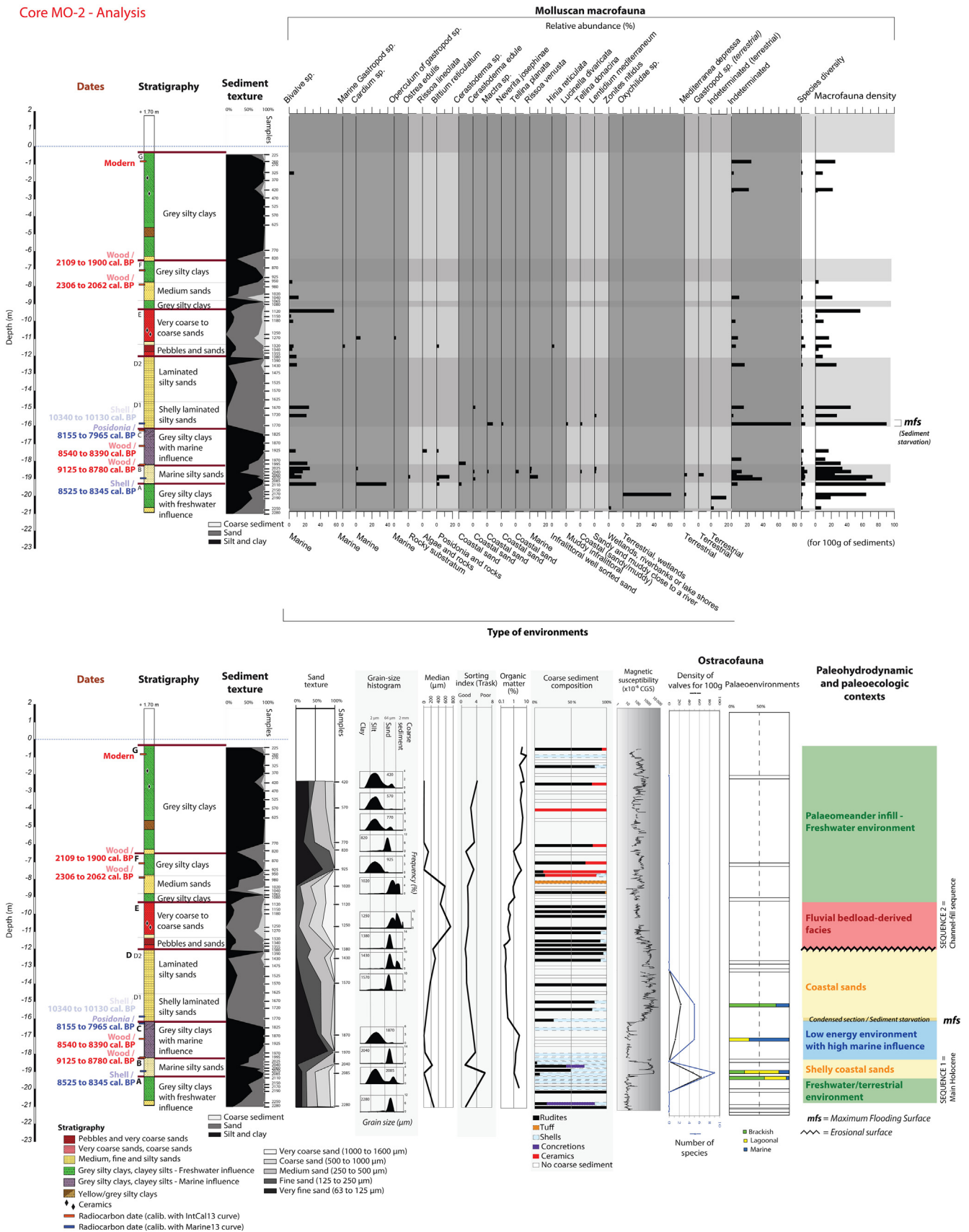
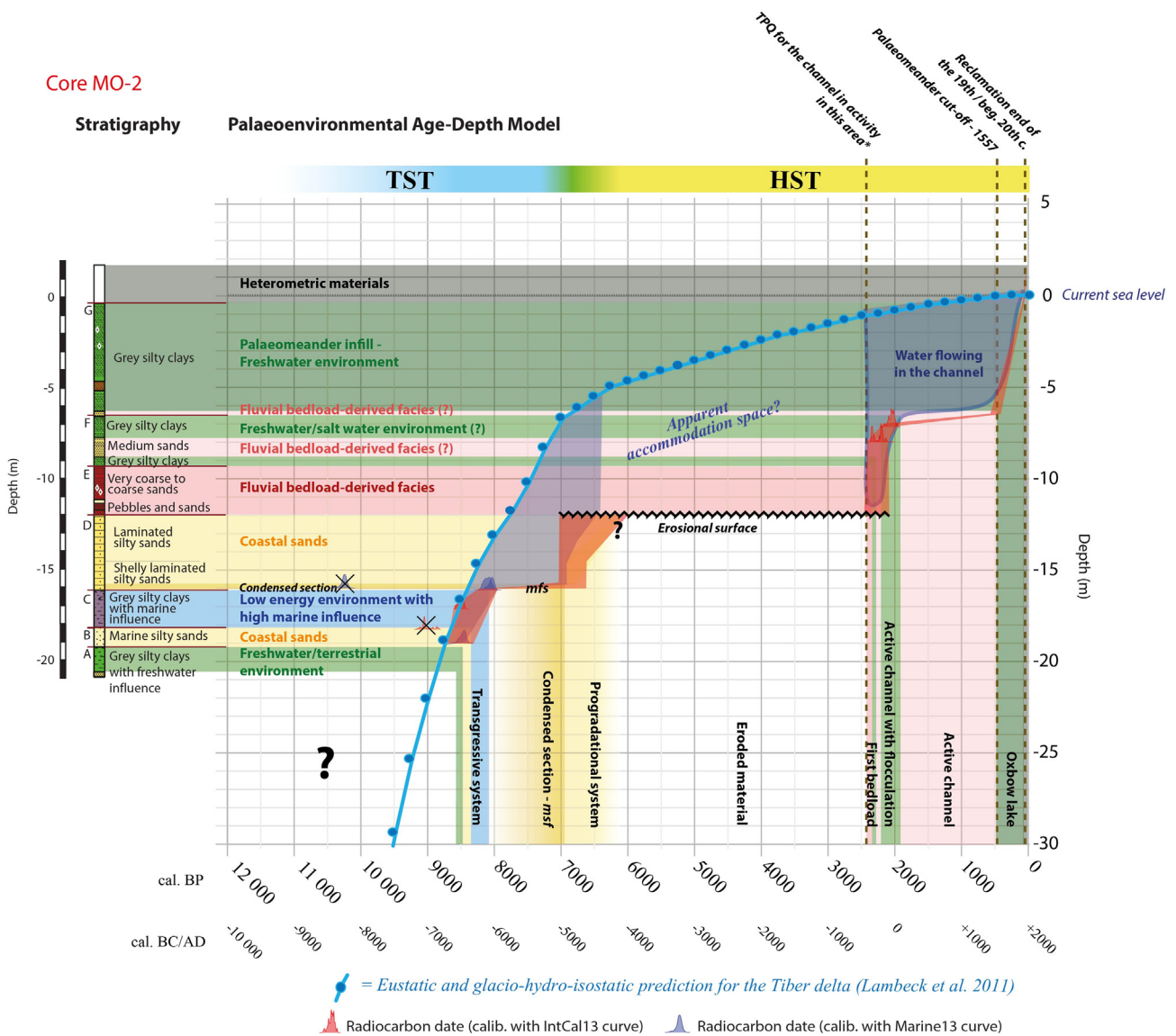


Fig. 8. Sedimentological and palaeoenvironmental analyses of Core MO-2.

Core MO-2



* see Salomon et al., 2017 for the discussion regarding the possible erosion of the Via Ostiensis by the palaeomeander of Ostia between 2500 and 1500 cal. BP

Fig. 9. PADM chart of Core MO-2.

The stratigraphic sequence of Core PO-2 records both the transition from the delta front to the prodelta during the transgression phase, and the transition from the prodelta to the prograded plain after the sea level rise slows down around 7000 yr ago. The coastal sands identified at the bottom of Core PO-2 might coincides with dates obtained in the TST deposits inland, pre-dating 7000 cal. BP. No dates are available for Unit A but we estimate that these transgressive coastal sands were deposited around 10,000 and 9000 cal. BP relying on the local sea level curve proposed by Lambeck et al. (2011). Sub-unit B1 shows the transition from the delta front (Unit A) to the prodelta (Unit B and C) while the coastline should be moving towards the east near Core MO-2 (retrogradation). The water-filled space (accommodation space) expands quickly right after the coastline in Core PO-2 is transgressed, but tends to reduce when the sea level rise slows down and the progradation occurs. Even if part of the slow sedimentation observed in Units B and C is because of compaction, such geometry and temporal evolution are expected in this geomorphological context. The mfs facies might also occur during this period (Unit B2). Units B to D expose the transition from the prodelta to the delta front while the Tiber delta plain is prograding. Sub-unit C1 records the first sandy layers since Sub-unit

B1 was deposited in the Early Holocene. Interestingly, freshwater ostracods species were identified in Sub-unit C1 along with brackish, coastal, and marine species. According to these palaeoenvironmental data and chronology obtained, a prograding palaeoriver mouth of the Tiber was most likely not far from Core PO-2 between 4500 and 4200 cal. BP. However, a stronger delta front influence is recorded just afterwards in Sub-unit C2. The delta front definitely progrades towards PO-2 between 4000 and 2500 cal. BP according to Unit D. The higher sedimentation rate in the upper level of Unit C and Unit D is probably because of less compaction but also to local factors linked to the closer coastline and adjustment of the slope of the delta front. This Sub-unit C2 could be related to the period of drier conditions between 4300 and 3800 cal. BP with intercalated phases of increased moisture recorded in lakes from Central Italy (Magny et al., 2007, 2009, 2012; Sadori et al., 2011). Similar progradational phases are also recorded in the Ombrone River delta (Bellotti et al., 2004). Anthropogenic factors, especially stronger human impact in the watershed, also most likely affected this coastal progradation from 4400 cal. BP (Bronze Age - Magri, 1999; Sadori et al., 2011). More ostracods usually living in freshwater were observed in Unit D suggesting closer river influence in this coastal area. According

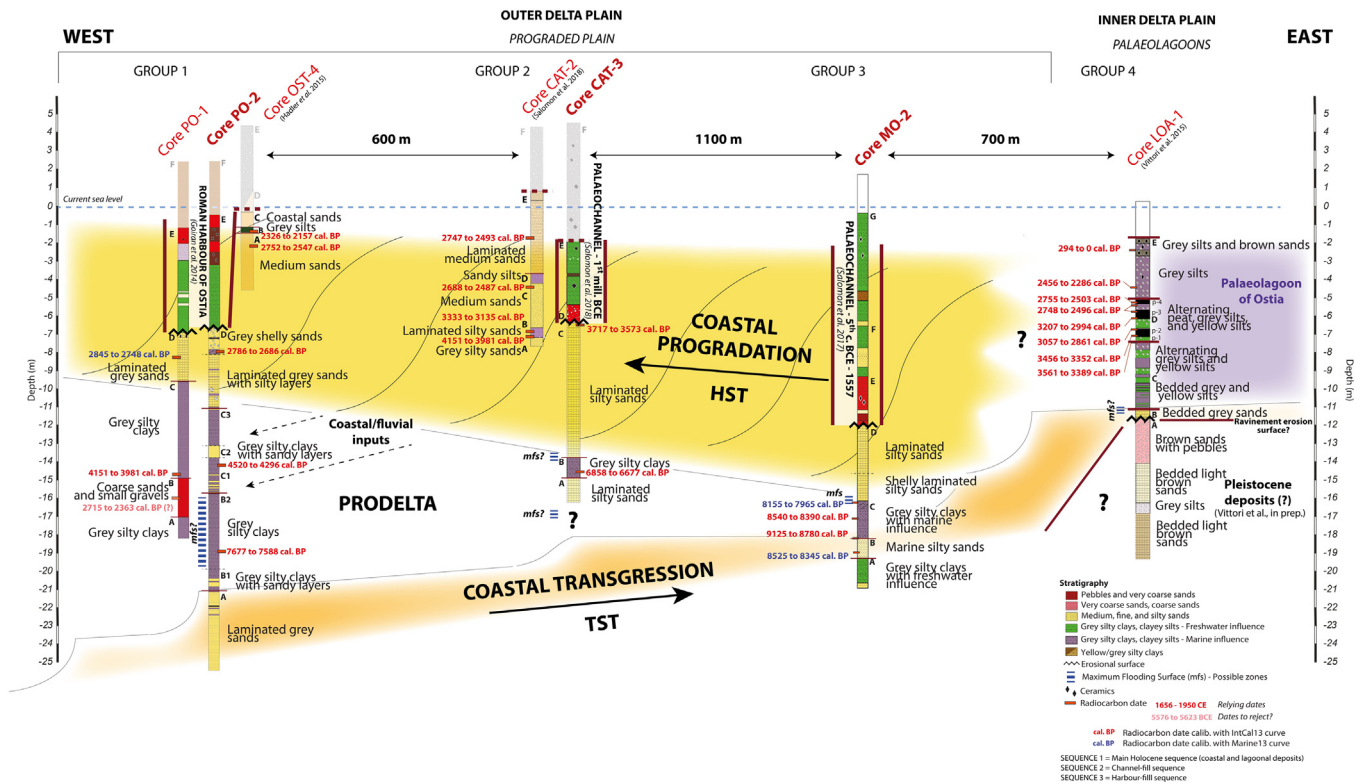


Fig. 10. Cross section of sedimentary cores drilled in the neighboring area of Ostia from the Roman palaeo-river mouth to the palaeolagoon of Ostia (new data and published data from Goiran et al., 2014; Vittori et al., 2015; Salomon et al., 2017, 2018).

to Core OST-4 (Hadler et al., 2015), the area of Core PO-2 definitely turns into the subaerial deltaic plain between 2.8 k and 2.5 k cal. BP.

5.3. Integrated age-depth model and interpretations

Fig. 11 is a synthesis of all of the apparent sedimentation curves from the cores drilled along the studied cross section from the archaeological site of Ostia to the palaeolagoon. This diagram integrates all of the PADMs presented above. Subsidence may have affected the sedimentation curve of the Outer subzone (Group 1) more than the curves of Inner subzone (Group 2 and 3), because of a deeper Holocene sequence to the west (see the unconformity at the base of the Tiber Depositional Sequence - Milli et al., 2013) and the thicker fine prodelta deposits recorded in Cores PO-1 and 2. However, despite the lack of dates at the bottom of each core, this chart confirms the succession of transgressed coastlines from west to east. The first coastline to be transgressed is in Group 1 (Core PO-2 - Outer subzone), then Group 2 (Core CAT-3), and finally Group 3 (Core MO-2 - Inner subzone). Consequently, the apparent accommodation space for the Outer subzone is deeper than for the Inner subzone between 8000 and 3000 cal. BP. This difference is also partly related to a higher subsidence in the Outer subzone. The apparent sedimentation rate is very low between 8000 and 4000 cal. BP in the Outer subzone, and accelerates since 4000 cal. BP to the definitive progradation of the Outer subzone (Group 1) around 2800–2700 cal. BP. This quicker sedimentation rate observed from 4000 cal. BP can be related to the lower compaction of these sandier layers, but also to delta front progradation in the Outer subzone. Additionally, it can also be a response to the aridification and stronger erosion happening across the Mediterranean since 4.2 k cal. BP.

The apparent sedimentation curves in the upper parts are a combination by groups of cores. Several radiocarbon dates were rejected to produce coherent sedimentation curves for each group and are crossed out on the diagram. Deepest and more recent radiocarbon dates were generally selected to plot the sedimentation curve (especially for

Cores CAT-2 and 3). When dates were very close in date and depth, we combined them within the sedimentation curve (Cores PO-1, PO-2 and OST-4). However, for the deepest date performed in Core PO-1/UnitB we adopted a different strategy because of the possible effect of the river, and two scenarios may be considered for now (see Discussion below). In any case, it results in a meeting of the sedimentation curves of Groups 1 and 2 around 2.8–2.5 k cal. BP. This observation confirms the quick progradation happening at that period (Salomon et al., 2018). Unfortunately, the HST coastline related to Core MO-2 is not known because of the erosion of the sediment from the upper part of the core by the palaeomeander of Ostia.

Considering (1) the succession of transgressed coastline from west to east observed in the integrated age-depth model (retrogradation), (2) the slower sedimentation in the prodelta comparing to the delta front, and (3) the sandy deposits reaching the modelled sea level curve during the HST (progradation), the model proposed fits into theoretical trends expected from a Holocene transgressed/prograded coast (see also Stanley and Warne, 1994; Tamura et al., 2003; Tanabe et al., 2006). The PADM chart seems relevant to identify evidence to reconstruct coastline-trajectories. The distinction between the apparent sedimentation curve of Groups 1, 2, and 3 might be amplified by the effect of compaction, but does not reassess the model proposed. Additionally, no strong chrono-topographical inversions suggest faulting activity below Ostia. This is confirmed by the fact that the dates in the lower part of Core MO-2 match the trend of evolution of the modelled local sea level curve. This approach considering geomorphological processes and their effect on sedimentation could contribute to improve decompaction methods for Late Pleistocene/Holocene deltaic sequences.

5.4. Fluvial bedload-derived facies within coastal sand near Ostia

The cross section presented in Fig. 10 shows the presence of facies interpreted such as fluvial bedload-derived deposit in very different

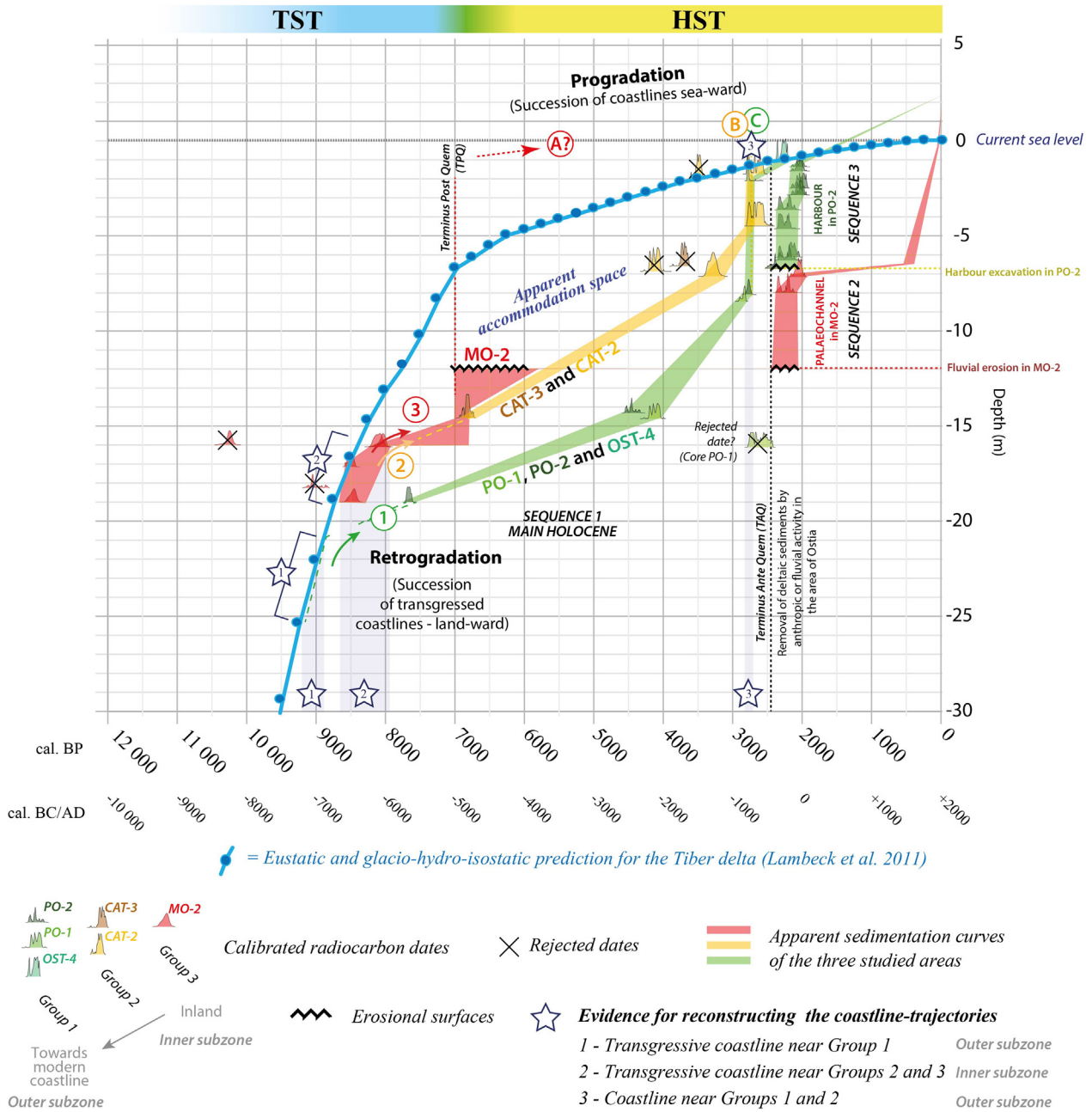


Fig. 11. Synthetic PADM chart for the final transgression phase and progradation until the Roman period. Sedimentation curves were merged into three studied area: Group 1 in green-Roman harbour area (Cores PO-1, PO-2 and OST-4); Group 2 in yellow- Area of the *Castrum* of Ostia (Cores CAT-2 and 3); and Group 3- Area of the lobe of the palaeomeander of Ostia (Core MO-2). This diagram shows evidence to reconstruct coastline-trajectories. (For interpretation of the references to color in this figure legend, the reader is referred to the web version of this article.)

palaeoenvironmental contexts: (1) in the prodelta in Core PO-1/Unit B; (2) in the progradational delta front in Core MO-2/Unit E, CAT-3/Unit D; and (3) in the Roman harbour in Core PO-1 and 2 - upper part of Units E. The bedload-derived facies of the Tiber River in its delta results in a distinct facies, composed of medium/coarse black sand with gravels and pebbles. Similar bedload-derived facies were also found in the Roman *Portus* canals (Salomon et al., 2014, 2016b) and in Core ISF-1 at the river mouth of the Tiber between 2500 and 2000 cal. BP (Salomon et al., 2018). Indirect fluvial influence is recorded on the coast and in the palaeolagoon with bioindicators such as ostracods and macrofauna. For information, the current maximum depth of the Tiber channel in the delta can reach 12 m (Castellano and Colatosti, 2003).

Initially, only coarse fluvial deposits from fluvial bedload-derived facies were assured to be found in the palaeomeander of

Ostia (Core MO-1, 2 and 3). The aerial photography taken in 1911 by balloon and sixteenth-seventeenth century texts and maps clearly revealed the position of the palaeomeander cut-off in 1557–1562 CE (Shepherd, 2006; Pannuzi, 2009). Other bedload-derived deposits were drilled by chance since Core CAT-2 was covered by a thick archaeological layer within the Roman city of Ostia. The fluvial harbour of Ostia was supposed to reveal only fine harbour muds, and only fine prodelta deposits were expected in the lower part of Core PO-1.

The bedload-derived facies of Unit B from Core PO-1 is related to a strong progradation in either 4000 cal. BP or around 2800–2700 cal. BP. The date of this fluvial deposit depends on the acceptance or the rejection of the date of 2715–2365 cal. BP dated on organic matter sampled in this unit. First, it was quite surprising to

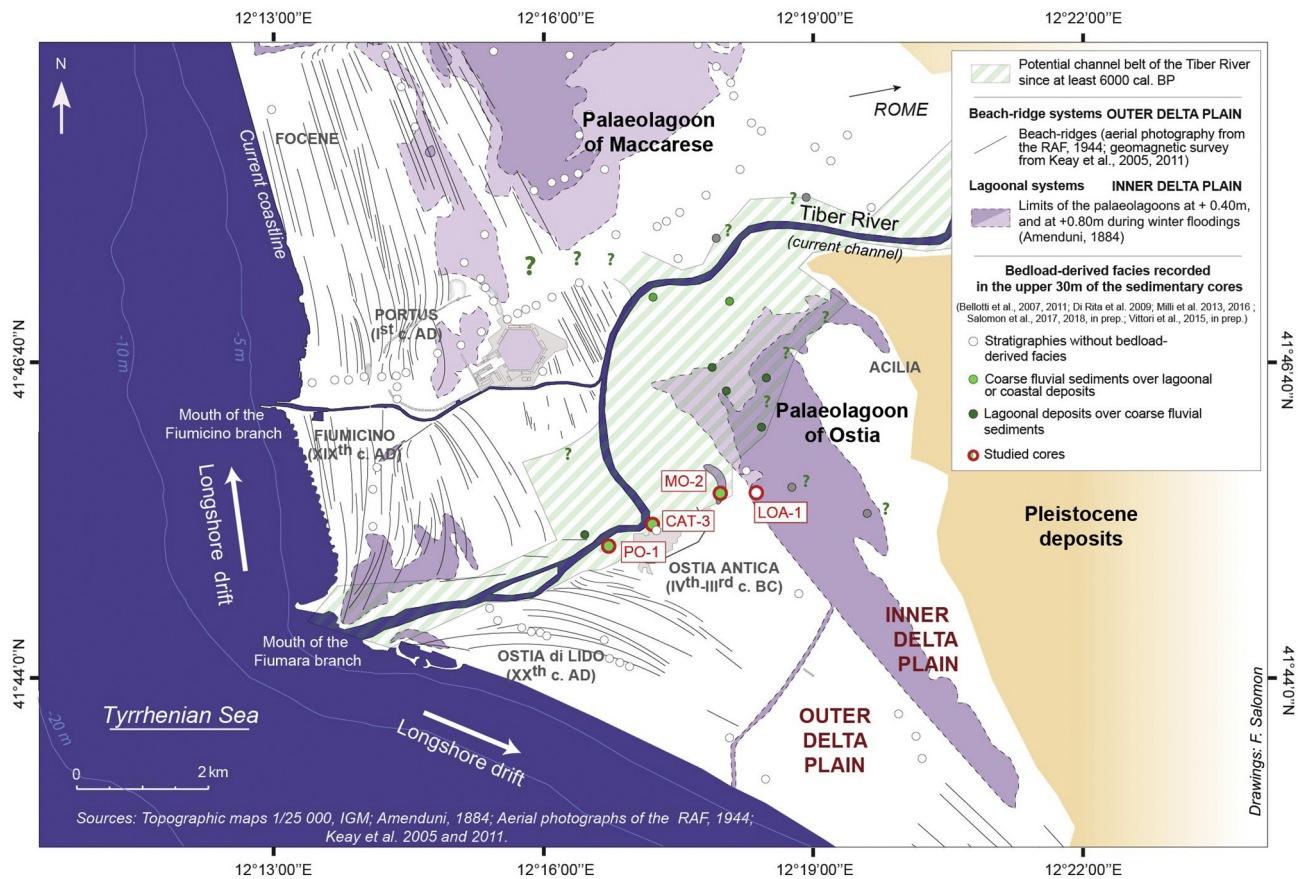


Fig. 12. Map of the possible channel belt of the Tiber in its delta for the last 6000 yr.

identify 2 m of coarse fluvial deposits between 15 and 17 m b.s.l. between two units of grey silty clay. This seems to be related to a quick and strong fluvial event. Second, Core PO-2 (located only 20 m away from Core PO-1) does not record a similar deposit. However, in Core PO-2/Sub-unit C1 around 15 m b.s.l. combined with the sandy layers deposited in the prodelta, few ostracods characteristic of a freshwater environment were identified. Third, the date of the bedload influx is similar to the quick progradation of 2800–2700 cal. BP recorded at the mouth of the Tiber delta (Salomon et al., 2018), but the date just on top could be related to the 4.2 k BP event (Magny et al., 2007; Sadori et al., 2011). Consequently, if the date is rejected, this bedload-derived deposit in PO-1/UnitB could be attributed to 4500–4000 cal. BP and be coeval with PO-2/Unit C. Alternatively, if the date of 2715–2363 cal. BP is accepted, this bedload-derived deposit would be part of the major change happening at the mouth of the Tiber River at 2800–2700 cal. BP.

The very coarse material issued from the bedload-derived deposit in the palaeomeander of Ostia in Core MO-2/UnitE was supposed to originate from the *Ponte Galeria* formation upstream of the Tiber delta and brought by a strong flood event (Salomon et al., 2017). The re-interpretation of the lower part of Core LOA-1/UnitA suggests that it could also belong to outcrops of Pleistocene deposits buried a few metres below the palaeolagoon of Ostia (Vittori et al. in prep.). Some pebbles from the Pleistocene outcrops could have been more locally eroded and trapped in the pool drilled in MO-2. The bedload-derived deposit found in Core CAT-3/UnitD is related to the palaeodynamic of the same palaeomeander of Ostia (Salomon et al., 2018). More surprising are the coarse deposits settled high over the sediment of the harbour of Ostia (Goiran et al., 2014). Their deposition in such a position could suggest shoals at the mouth of the Tiber River around 2000 cal. BP.

5.5. Tiber river mobility in the Tiber delta during the last 6000 years cal. BP

The last figure is a map of the lateral mobility of the Tiber River during the last 6000 yr in its delta with data available for now (Fig. 12). This timespan covers most of the period of the HST and the progradation of the Tiber delta. Several data have been collected to produce this map: (1) beach ridge and fluvial features observed in satellite imagery, old aerial photography, and geophysical surveys (Keay et al., 2005; Keay and Paroli, 2011); and (2) stratigraphic sequences with coarse fluvial deposits. Only the upper 30 m of the cores were considered. Beach ridge features are important data because they express progradation phases not removed by river mobility. The limit of this indicator is in cases of strong coastal erosion. In this case, stratigraphic sequences can be of great help. This dataset is completed by the new data published in this paper.

Recently, several papers suggested the existence of a palaeochannel of the Tiber below the Roman harbour of Portus between 3000 and 2400 cal. BP and a strong avulsion towards the south (Giraudi et al., 2009). However, for now no clear evidence of bedload-derived deposits supports such a hypothesis. Data from Cores PO-1 and 2 demonstrate that a branch of the Tiber River in the southern side of the delta existed since 4500–4000 cal. BP. Nevertheless, an area void of surficial features and sedimentary drilling remains between the southern part of the International airport of Fiumicino and the north of the harbour of the Roman emperor Trajan (Fig. 1).

Most of the coarse fluvial deposits identified in the upper 30 m of the cores were drilled in the northern part of the Palaeolagoon of Ostia and the current Tiber (Bellotti et al., 2007). Cores drilled at Ostia, especially Cores CAT-2 and CAT-3, expose a clear southern limit for the fluvial mobility of the Tiber during the Late Holocene. Less clear is the central and southern part of the palaeolagoon of Ostia. Finally, a recent magnetic survey conducted in the Isola Sacra revealed fluvial features in the

southern part (Germoni et al., 2018; Keay, Strutt et al. in prep.). A migration of the Tiber from the middle of the Isola Sacra to Ostia could have occurred in the between 2800 and 1700 cal. BP. During the last 2000 yr, the lateral mobility of the Tiber in the new prograded delta plain was mainly constrained along the Fiumara. The main change seems to be related to the cut-off of the Tiber River near Ostia and the construction of the Roman canals, including the Fiumicino.

6. Conclusion

This paper demonstrates that PADM charts (Palaeoenvironmental Age-Depth Models) are very well adapted to interpret deltaic stratigraphic sequences and to distinguish transgressive and progradational sequences. During the Early Holocene, the transgression of the coastline from east to west is clearly observed in the studied cross section. Single and combined PADM charts for different groups of cores also expose the different progradation phases affecting the Tiber delta. The integration of different apparent sedimentation curves in a single age-depth model demonstrates the effect of the sedimentation context (e.g., higher sedimentation rates in the delta front comparing to the prodelta) and clearly expose the succession of transgressed and prograded coastlines during the Holocene. It gives clear evidence to reconstruct coastline-trajectories. This integrated model could contribute to adjust decompaction methods for deltaic sequences.

Within the PADM chart, fluvial mobility makes the interpretations more complex. River dynamics erode part of the coastal stratigraphic sequences. Nevertheless, the PADM chart produces a clear view of the palaeoenvironmental context in which fluvial sediments are deposited (prodelta/delta front, incision/deposition). It also exposes the relation between the fluvial deposits and the modelled sea level curve. Indirect evidence of fluvial activity based on bioindicators (freshwater influence) recorded in the prodelta or delta front are very informative. They suggest that the Tiber flowed towards the south of its delta from 4500 to 4200 cal. BP. Additionally, the Tiber bedload-derived facies recorded in the prodelta reveals complex depositional processes and interplays between the river and the delta formation.

The reconstruction of the coastal and fluvial mobility in deltaic contexts during the Holocene remains a difficult task. The reconstruction of the Holocene relative sea level curves remains one of the most important data in producing reliable interpretations. A more detailed and less smoothed modelled relative sea level curve is essential and would bring more reliable interpretations. This is particularly true to study the consequence of the sea level jumps between 9000 and 8000 cal. BP on coastal depositional contexts.

Declaration of competing interest

The authors declare that they have no known competing financial interests or personal relationships that could have appeared to influence the work reported in this paper.

Acknowledgments

We gratefully acknowledge financial and logistical support of the École française de Rome and the British School at Rome, as well as financial support from ANR-Poltevere (ANR-11-JSH3-0002) and from the European Research Council under the European Union's Seventh Framework Programme (FP7/2007-2013)/ERC grant agreement n°339123. We would also like to thank the *Soprintendenza Speciale Archeologia Belle Arti e Paesaggio di Roma* and the *Parco Archeologico di Ostia Antica*. A thank you to Leah Holguin for proofreading the English text.

References

Allen, P.A., Allen, J.R., 2013. *Basin Analysis: Principles and Application to Petroleum Play Assessment*. John Wiley & Sons.

- Amenduni, G., 1884. *Sulle opere di bonificazione della plaga litoranea dell'Agro Romano che comprende le paludi e gli stagni di Ostia, Porto, Maccarese e delle terre vallive di Stracciappia, Baccano, Pantano e Lago dei Tartari*. Relazione del progetto generale 15, 36.
- Amorosi, A., Milli, S., 2001. Late Quaternary depositional architecture of Po and Tevere river deltas (Italy) and worldwide comparison with coeval deltaic successions. *Sediment. Geol.* 144, 357–375.
- Amorosi, A., Bruno, L., Campo, B., Morelli, A., Rossi, V., Scarponi, D., Hong, W., Bohacs, K.M., Drexler, T.M., 2017. Global sea-level control on local parasequence architecture from the Holocene record of the Po Plain, Italy. *Mar. Pet. Geol.* <https://doi.org/10.1016/j.marpetgeo.2017.01.020>.
- Anthony, E.J., Marriner, N., Morhange, C., 2014. Human influence and the changing geomorphology of Mediterranean deltas and coasts over the last 6000 years: from progradation to destruction phase? *Earth Sci. Rev.* 139, 336–361. <https://doi.org/10.1016/j.earscirev.2014.10.003>.
- Arnoldus-Huyzendveld, A., Paroli, L., 1995. Alcune considerazioni sullo sviluppo storico dell'ansa del Tevere presso Ostia e sul porto-canale. *Archeologia Laziale* 12, 383–392.
- Arnoldus-Huyzendveld, A., Pellegrino, A., 1999. Traces of historical landscapes preserved in the coastal area of Rome. *Memorie Descrittive della Carta Geologica d'Italia* 65, 219–226.
- Autorità di Bacino del Fiume Tevere, 2006. *Il Tevere a Roma-Portolano*. Edizioni Ambiente, Milano.
- Belfiore, A., Bellotti, P., Carboni, M.G., Chiari, R., Evangelista, S., Tortora, P., Valeri, P., 1987. Il delta del Tevere: le facies sedimentarie della conoide sommersa. Un'analisi statistica dei caratteri tessiturali, microfaunistici e mineralogici. *Boll. Soc. Geol. It.* 106, 425–445.
- Bellan-Santini, D., Lacaze, J.C., Poizat, C., Pérès, J.M., 1994. Les biocénoses marines et littorales de Méditerranée, synthèse, menaces et perspectives. *Collection patrimoines naturels* 19, 246.
- Bellotti, P., Carboni, M.G., Milli, S., Tortora, P., Valeri, P., 1989. La piana delizia del Fiume Tevere: analisi di facies ed ipotesi evolutiva dell'ultimo "low stand" glaciale all'attuale. *Giorn. Geol.* 51, 71–91.
- Bellotti, P., Chiocci, F.L., Milli, S., Tortora, P., Valeri, P., 1994. Sequence stratigraphy and depositional setting of the Tiber delta: integration of high-resolution seismics, well logs, and archeological data. *Journal of Sedimentary Research-Section B-Stratigraphy and Global Studies* 64, 416–432.
- Bellotti, P., Milli, S., Tortora, P., Valeri, P., 1995. Physical stratigraphy and sedimentology of the Late Pleistocene-Holocene Tiber Delta depositional sequence. *Sedimentology* 42, 617–634.
- Bellotti, P., Caputo, C., Davoli, L., Evangelista, S., Garzanti, E., Pugliese, F., Valeri, P., 2004. Morpho-sedimentary characteristics and Holocene evolution of the emergent part of the Ombrone River delta (southern Tuscany). *Geomorphology, Hazards of Mass Movements* 61, 71–90. <https://doi.org/10.1016/j.geomorph.2003.11.007>.
- Bellotti, P., Calderoni, G., Carboni, M.G., Di Bella, L., Tortora, P., Valeri, P., Zernitskaya, V., 2007. Late Quaternary landscape evolution of the Tiber River delta plain (Central Italy): new evidence from pollen data, biostratigraphy and 14C dating. *Z. Geomorphol.* 51, 505–534.
- Bellotti, P., Calderoni, G., Di Rita, F., D'Orefice, M., D'Amico, C., Esu, D., Magri, D., Martinez, M.P., Tortora, P., Valeri, P., 2011. The Tiber river delta plain (central Italy): coastal evolution and implications for the ancient Ostia Roman settlement. *The Holocene* 21, 1105–1116. <https://doi.org/10.1177/0959683611400464>.
- Bellotti, P., Davoli, L., Sadori, L., 2018. Landscape diachronic reconstruction in the Tiber delta during historical time: a holistic approach. *Geogr. Fis. Din. Quat.* 41, 3–21.
- Belluomini, G., Iuzzolini, P., Manfra, L., Mortari, R., Zalaffi, M., 1986. *Evoluzione recente del delta del Tevere*. *Geol. Romana* 25, 213–234.
- Bersani, P., Bencivenga, M., 2001. *Le Piene del Tevere a Roma dal V secolo a.C. all'anno 2000*, Servizio Idrografico e Mareografico Nazionale. ed. Presidenza del Consiglio dei Ministri Dipartimento per i Servizi Tecnici Nazionali, Rome.
- Bersani, P., Moretti, D., 2008. Evoluzione storica della linea di costa in prossimità della foce del Tevere. *L'Acqua* 5, 77–88.
- Bicket, A.R., Rendell, H.M., Claridge, A., Rose, P., Andrews, J., Brown, F.S.J., 2009. A multiscale geoaerchaeological approach from the Laurentine shore (Castelporziano, Lazio, Italy). *Géomorphologie: Relief. Processus. Environnement* 4, 257–270.
- Bigi, S., Beaubien, S.E., Ciotoli, G., D'Ambrogio, C., Doglioni, C., Ferrante, V., Lombardi, S., Milli, S., Orlando, L., Ruggiero, L., Tartarello, M.C., Sacco, P., 2014. Mantle-derived CO₂ migration along active faults within an extensional basin margin (Fiumicino, Rome, Italy). *Tectonophysics* 637, 137–149. <https://doi.org/10.1016/j.tecto.2014.10.001>.
- Bradford, J., 1957. *Ancient Landscapes. Studies in Field Archaeology*. G. Bell, London.
- Bruno, L., Amorosi, A., Severi, P., Costagli, B., 2017. Late Quaternary aggradation rates and stratigraphic architecture of the southern Po Plain, Italy. *Basin Res.* 29, 234–248. <https://doi.org/10.1111/br.12174>.
- Cailleux, A., Tricart, J., 1959. *Initiation à l'étude des sables et des galets*. Centre de documentation universitaire, Paris.
- Carbonel, P., 1988. Ostracods and the transition between fresh and saline waters. In: De Deckker, P., Colin, J.-P., Peyrrouquet, J.-P. (Eds.), *Ostracoda in the Earth Sciences*, pp. 157–173.
- Castellano, F., Colatosti, G., 2003. I rilievi topografici dell'alveo del Tevere nell'area metropolitana romana. *Tevere* 23–24 (80–73).
- Catuneanu, O., 2006. *Principles of Sequence Stratigraphy*. Elsevier.
- Catuneanu, O., Abreu, V., Bhattacharya, J.P., Blum, M.D., Dalrymple, R.W., Eriksson, P.G., Fielding, C.R., Fisher, W.L., Galloway, W.E., Gibling, M.R., et al., 2009. Towards the standardization of sequence stratigraphy. *Earth Sci. Rev.* 92, 1–33.
- Cearreta, A., Benito, X., Ibáñez, C., Trobajo, R., Giosan, L., 2016. Holocene palaeoenvironmental evolution of the Ebro Delta (Western Mediterranean Sea): evidence for an early construction based on the benthic foraminiferal record. *The Holocene* 26, 1438–1456. <https://doi.org/10.1177/0959683616640048>.

- Ciotoli, G., Etiope, G., Marra, F., Florindo, F., Giraudi, C., Ruggiero, L., 2016. Tiber delta CO₂-CH₄ degassing: a possible hybrid, tectonically active Sediment-Hosted Geothermal System near Rome. *J. Geophys. Res. Solid Earth* 121, 2015JB012557. <https://doi.org/10.1002/2015JB012557>.
- Coleman, J.M., 1982. *Deltas: Processes of Deposition & Models for Exploration*. International Human Resources Development Corporation, Boston.
- De Lange, G.J., Thomson, J., Reitz, A., Slomp, C.P., Principato, M.S., Erba, E., Corselli, C., 2008. Synchronous basin-wide formation and redox-controlled preservation of a Mediterranean sapropel. *Nat. Geosci.* 1, 606–610. <https://doi.org/10.1038/ngeo283>.
- De Rita, D., Bertagnini, A., Carboni, G., Ciccacci, S., Di Filippo, M., Faccenna, C., Fredi, P., Funicello, R., Landi, P., Sciacca, P., 1994. Geological-petrological evolution of the Ceriti Mountains area (Latium, central Italy). *Mem Des Carta Geol It* 49, 291–322.
- Dearing, J.A., 1999. Environmental magnetic susceptibility. Using the Bartington MS2 System 32, 54.
- Dragone, F., Mano, A., Malatesta, A., Segre, A., 1967. Note illustrative del Foglio 149 Cerveteri della Carta Geologica d'Italia. Servizio Geologico d'Italia 4, 1–93.
- Embry, A., Johannessen, E., Owen, D., Beauchamp, B., Gianolla, P., 2007. Sequence stratigraphy as a "concrete" stratigraphic discipline. Report of the ISSC Task Group on sequence stratigraphy 1, 104.
- Emeis, K.-C., Struck, U., Schulz, H.-M., Rosenberg, R., Bernasconi, S., Erlenkeuser, H., Sakamoto, T., Martinez-Ruiz, F., 2000. Temperature and salinity variations of Mediterranean Sea surface waters over the last 16,000 years from records of planktonic stable oxygen isotopes and alkenone unsaturation ratios. *Palaeogeogr. Palaeoclimatol. Palaeoecol.* 158, 259–280. [https://doi.org/10.1016/S0031-0182\(00\)00053-5](https://doi.org/10.1016/S0031-0182(00)00053-5).
- Ferranti, L., Antonioli, F., Mauz, B., Amorosi, A., Dai Pra, G., Mastronuzzi, G., Monaco, C., Orr, P., Pappalardo, M., Radtke, U., Renda, P., Romano, P., Sanso, P., Verrubbi, V., 2006. Markers of the last interglacial sea-level high stand along the coast of Italy: tectonic implications. *Quat. Int.* 145–46, 30–54.
- Folk, R.L., Ward, W.C., 1957. Brazos River bar [Texas]; a study in the significance of grain size parameters. *J. Sediment. Res.* 27, 3–26.
- Frenzel, P., Boomer, I., 2005. The use of ostracods from marginal marine, brackish waters as bioindicators of modern and Quaternary environmental change. *Palaeogeogr. Palaeoclimatol. Palaeoecol.* 225, 68–92. <https://doi.org/10.1016/j.palaeo.2004.02.051>.
- Funicello, R., 1995. *La geologia di Roma. Il centro storico. Memorie descrittive della Carta Geologica d'Italia, Servizio Geologico Nazionale* 50.
- Gebremichael, E., Sultan, M., Becker, R., El Bastawesy, M., Cherif, O., Emil, M., 2018. Assessing land deformation and sea encroachment in the Nile Delta: a radar interferometric and inundation modeling approach. *J. Geophys. Res. Solid Earth* 123, 3208–3224.
- Germoni, P., Keay, S., Millett, M., Strutt, K., 2018. Ostia beyond the Tiber: recent archaeological discoveries in the Isola Sacra. In: Cèbeillac-Gervasoni, M., Laubry, N., Zevi, F. (Eds.), *Ricerche Su Ostia e Il Suo Territorio: Atti Del Terzo Seminario Ostiense (Roma, École Française de Rome, 21–22 Ottobre 2015)*, Collection de l'École Française de Rome. Publications de l'École française de Rome, Rome.
- Giraudi, C., 2004. Evoluzione tardo-olocenica del delta del Tevere. *Il Quaternario* 17, 477–492.
- Giraudi, C., Tata, C., Paroli, L., 2009. Late Holocene evolution of Tiber river delta and geoarchaeology of Claudius and Trajan Harbor, Rome. *Geoarchaeology* 24, 371–382. <https://doi.org/10.1002/gea.20270>.
- Goiran, J.-P., 2001. *Recherches géomorphologiques dans la région littorale d'Alexandrie en Egypte*. (PhD thesis in Physical Geography). Université de Provence, Aix-en-Provence.
- Goiran, J.-P., Tronchère, H., Salomon, F., Carbonel, P., Djerbi, H., Ognard, C., 2010. Palaeoenvironmental reconstruction of the ancient harbors of Rome: Claudius and Trajan's marine harbors on the Tiber delta. *Quat. Int.* 216, 3–13. <https://doi.org/10.1016/j.quaint.2009.10.030>.
- Goiran, J.-P., Salomon, F., Tronchère, H., Djerbi, H., Carbonel, P., Ognard, C., Oberlin, C., 2011. Géographie des ports de Claude et de Trajan, Portus, delta du Tibre. *MEFRA-Antiquité* 123, 157–236. <https://doi.org/10.4000/mefra.491>.
- Goiran, J.-P., Salomon, F., Mazzini, I., Bravard, J.-P., Pleuger, E., Vittori, C., Boetto, G., Christiansen, J., Arnaud, P., Pellegrino, A., Pepe, C., Sadori, L., 2014. Geoarchaeology confirms location of the ancient harbour basin of Ostia (Italy). *J. Archaeol. Sci.* 41, 389–398. <https://doi.org/10.1016/j.jas.2013.08.019>.
- Hadler, H., Fischer, P., Obrocki, L., Heinzlmann, M., Vött, A., 2020. River channel evolution and tsunami impacts recorded in local sedimentary archives – the 'Fiume Morto' at Ostia Antica (Tiber River, Italy). *Sedimentology* 67 (3), 1309–1343. <https://doi.org/10.1111/sed.12599>.
- Hadler, H., Vött, A., Fischer, P., Ludwig, S., Heinzlmann, M., Rohn, C., 2015. Temple-complex post-dates tsunami deposits found in the ancient harbour basin of Ostia (Rome, Italy). *J. Archaeol. Sci.* 61, 78–89. <https://doi.org/10.1016/j.jas.2015.05.002>.
- Heiri, O., Lotter, A.F., Lemcke, G., 2001. Loss on ignition as a method for estimating organic and carbonate content in sediments: reproducibility and comparability of results. *J. Paleolimnol.* 25, 101–110. <https://doi.org/10.1023/A:1008119611481>.
- Hijma, M.P., Cohen, K.M., 2011. Holocene transgression of the Rhine river mouth area, The Netherlands/Southern North Sea: palaeogeography and sequence stratigraphy. *Sedimentology* 58, 1453–1485. <https://doi.org/10.1111/j.1365-3091.2010.01222.x>.
- Hijma, M.P., Cohen, K.M., 2019. Holocene sea-level database for the Rhine-Meuse Delta, The Netherlands: implications for the pre-8.2 ka sea-level jump. *Quat. Sci. Rev.* 214, 68–86. <https://doi.org/10.1016/j.quascirev.2019.05.001>.
- Hori, K., Saito, Y., 2007. An early Holocene sea-level jump and delta initiation. *Geophys. Res. Lett.* 34.
- Johnson, C.S., Miller, K.G., Browning, J.V., Kopp, R.E., Khan, N.S., Fan, Y., Stanford, S.D., Horton, B.P., 2018. The role of sediment compaction and groundwater withdrawal in local sea-level rise, Sandy Hook, New Jersey, USA. *Quat. Sci. Rev.* 181, 30–42. <https://doi.org/10.1016/j.quascirev.2017.11.031>.
- Karner, D.B., Marra, F., Florindo, F., Boschi, E., 2001a. Pulsed uplift estimated from terrace elevations in the coast of Rome: evidence for a new phase of volcanic activity? *Earth Planet. Sci. Lett.* 188, 135–148. [https://doi.org/10.1016/S0012-821X\(01\)00325-9](https://doi.org/10.1016/S0012-821X(01)00325-9).
- Karner, D.B., Marra, F., Renne, P.R., 2001b. The history of the Monti Sabatini and Alban Hills volcanoes: groundwork for assessing volcanic-tectonic hazards for Rome. *J. Volcanol. Geotherm. Res.* 107, 185–215. [https://doi.org/10.1016/S0377-0273\(00\)00258-4](https://doi.org/10.1016/S0377-0273(00)00258-4).
- Keay, S., Paroli, L., 2011. *Portus and Its Hinterland: Recent Archaeological Research*, Archaeological Monographs of the British School at Rome. British School at Rome, London.
- Keay, S., Millett, M., Paroli, L., Strutt, K., 2005. *Portus: An Archaeological Survey of the Portus of Imperial Rome*, Archaeological Monographs of the British School at Rome. British School at Rome, London.
- Kominz, M.A., Patterson, K., Odette, D., 2011. Lithology dependence of porosity in slope and deep marine sediments. *J. Sediment. Res.* 81, 730–742. <https://doi.org/10.2110/jsr.2011.60>.
- Lambeck, K., Antonioli, F., Anzidei, M., Ferranti, L., Leoni, G., Scicchitano, G., Silenzi, S., 2011. Sea level change along the Italian coast during the Holocene and projections for the future. *Quaternary International, Tectonic Contribution to Relative Sea Level Change* 232, 250–257. <https://doi.org/10.1016/j.quaint.2010.04.026>.
- Lambeck, K., Rouby, H., Purcell, A., Sun, Y., Sambridge, M., 2014. Sea level and global ice volumes from the Last Glacial Maximum to the Holocene. *PNAS* 111, 15296–15303. <https://doi.org/10.1073/pnas.1411762111>.
- Le Gall, J., 1953. *Le Tibre, fleuve de Rome dans l'antiquité*. Presses Universitaires de France, Paris.
- Magny, M., De Beaulieu, J.-L., Drescher-Schneider, R., Vannière, B., Walter-Simonnet, A.V., Miras, Y., Millet, L., Bossuet, G., Peyron, O., Brugiapaglia, E., et al., 2007. Holocene climate changes in the central Mediterranean as recorded by lake-level fluctuations at Lake Accesa (Tuscany, Italy). *Quat. Sci. Rev.* 26, 1736–1758.
- Magny, M., Vannière, B., Zanchetta, G., Fouache, E., Touchais, G., Petrika, L., Coussot, C., Walter-Simonnet, A.V., Arnaud, F., 2009. Possible complexity of the climatic event around 4300–3800 cal. BP in the central and western Mediterranean. *The Holocene* 19, 823–833. <https://doi.org/10.1177/0959683609337360>.
- Magny, M., Peyron, O., Sadori, L., Ortu, E., Zanchetta, G., Vannière, B., Tinner, W., 2012. Contrasting patterns of precipitation seasonality during the Holocene in the south- and north-central Mediterranean. *J. Quat. Sci.* 27, 290–296.
- Magri, D., 1999. Late Quaternary vegetation history at Lagaccione near Lago di Bolsena (central Italy). *Rev. Palaeobot. Palynol.* 106, 171–208. [https://doi.org/10.1016/S0034-6667\(99\)00006-8](https://doi.org/10.1016/S0034-6667(99)00006-8).
- Mantovani, E., Babbucci, D., Tamburelli, C., Viti, M., 2009. A review on the driving mechanism of the Tyrrhenian–Apennines system: implications for the present seismotectonic setting in the Central-Northern Apennines. *Tectonophysics* 476, 22–40. <https://doi.org/10.1016/j.tecto.2008.10.032>.
- Marra, F., Bozzano, F., Cinti, F.R., 2013. Chronostratigraphic and lithologic features of the Tiber River sediments (Rome, Italy): implications on the post-glacial sea-level rise and Holocene climate. *Glob. Planet. Chang.* 107, 157–176. <https://doi.org/10.1016/j.gloplacha.2013.05.002>.
- Marra, F., Milana, G., Pecchioli, L., Roselli, P., Cangi, G., Famiani, D., Mercuri, A., Carlucci, G., 2019. Historical faulting as the possible cause of earthquake damages in the ancient Roman port city of Ostia. *J. Seismol.* <https://doi.org/10.1007/s10950-019-09844-z>.
- Marriner, N., Morhange, C., Doumet-Serhal, C., 2006. *Geoarchaeology of Sidon's ancient harbours, Phoenicia*. *J. Archaeol. Sci.* 33, 1514–1535.
- Mazzini, I., Faranda, C., Giardini, M., Giraudi, C., Sadori, L., 2011. Late Holocene palaeoenvironmental evolution of the Roman harbour of Portus, Italy. *J. Paleolimnol.* 46, 243–256. <https://doi.org/10.1007/s10933-011-9536-7>.
- Milli, S., 1997. Depositional setting and high-frequency sequence stratigraphy of the Middle-Upper Pleistocene to Holocene deposits of the Roman Basin. *Geol. Romana* 33, 99–136.
- Milli, S., D'Ambrò, C., Bellotti, P., Calderoni, G., Carboni, M.G., Celant, A., Di Bella, L., Di Rita, F., Frezza, V., Magri, D., Pichezzi, R.M., Ricci, V., 2013. The transition from wave-dominated estuary to wave-dominated delta: the Late Quaternary stratigraphic architecture of Tiber River deltaic succession (Italy). *Sediment. Geol.* 284–285, 159–180. <https://doi.org/10.1016/j.sedgeo.2012.12.003>.
- Milli, S., Mancini, M., Moscatelli, M., Stigliano, F., Marini, M., Cavinato, G.P., 2016. From river to shelf, anatomy of a high-frequency depositional sequence: the Late Pleistocene to Holocene Tiber depositional sequence. *Sedimentology* <https://doi.org/10.1111/sed.12277> (n/a-n/a).
- Pannuzi, S., 2009. *Il Castello di Giulio II ad Ostia Antica, Documenti di archeologia postmedievale*. All'Insegna del Giglio, Firenze.
- Perès, J.M., Picard, J., 1964. *Nouveau manuel de biologie benthique de la Mer Méditerranée*. Rec. Trav. Station marine d'Endoume, Marseille.
- Posamentier, H.W., James, D.P., 1993. An overview of sequence-stratigraphic concepts: users and abuses. *Sequence stratigraphy and facies associations* 3–18.
- Pranzini, E., 2007. Airborne LiDAR survey applied to the analysis of the historical evolution of the Arno River delta (Italy). *J. Coast. Res.* 50, 400–409.
- Ramsey, C.B., 1995. Radiocarbon calibration and analysis of stratigraphy: the OxCal program. *Radiocarbon* 37, 425–430.
- Ramsey, C.B., Lee, S., 2013. Recent and planned developments of the program OxCal. *Radiocarbon* 55, 720–730.
- Reimer, P.J., Bard, E., Bayliss, A., Beck, J.W., Blackwell, P.G., Bronk Ramsey, C., Buck, C.E., Cheng, H., Edwards, R.L., Friedrich, M., Grootes, P.M., Guilderson, T.P., Hafflason, H., Hajdas, I., Hatté, C., Heaton, T.J., Hoffmann, D.L., Hogg, A.G., Hughen, K.A., Kaiser, K.F., Kromer, B., Manning, S.W., Niu, M., Reimer, R.W., Richards, D.A., Scott, E.M., Southon, J.R., Staff, R.A., Turney, C.S.M., van der Plicht, J., 2013. *IntCal13 and Marine13*

- radiocarbon age calibration curves 0–50, 000 years cal BP. *Radiocarbon* 55, 1869–1887.
- Ruiz, F., Abad, M., Bodergat, A.M., Carbonel, P., Rodríguez-Lázaro, J., Yasuhara, M., 2005. Marine and brackish-water ostracods as sentinels of anthropogenic impacts. *Earth Sci. Rev.* 72, 89–111. <https://doi.org/10.1016/j.earscirev.2005.04.003>.
- Sadori, L., Jahns, S., Peyron, O., 2011. Mid-Holocene vegetation history of the central Mediterranean. *The Holocene* 21, 117–129.
- Sadori, L., Mazzini, I., Pepe, C., Goiran, J.-P., Pleuger, E., Ruscito, V., Salomon, F., Vittori, C., 2016. Palynology and ostracodology at the Roman port of ancient Ostia (Rome, Italy). *The Holocene* 26, 1502–1512. <https://doi.org/10.1177/0959683616640054>.
- Salomon, F., 2013. *Géochronologie du delta du Tibre: Evolution géomorphologique holocène et contraintes hydrosédimentaires dans le système Ostie-Portus*. (Thèse de doctorat en Géographie Physique/Géochronologie). 2. Université Lyon.
- Salomon, F., Goiran, J.-P., Bravard, J.-P., Arnaud, P., Djerbi, H., Kay, S., Keay, S., 2014. A harbour–canal at Portus: a geoarchaeological approach to the Canale Romano: Tiber delta, Italy. *Water Hist* 6, 31–49. <https://doi.org/10.1007/s12685-014-0099-1>.
- Salomon, F., Keay, S., Carayon, N., Goiran, J.-P., 2016a. The development and characteristics of ancient harbours—applying the PADM chart to the case studies of Ostia and Portus. *PLoS ONE* 11, e0162587. <https://doi.org/10.1371/journal.pone.0162587>.
- Salomon, F., Keay, S., Strutt, K., Goiran, J.-P., Millett, M., Germoni, P., 2016b. Connecting Portus with Ostia: preliminary results of a geoarchaeological study of the navigable canal on the Isola Sacra. *Revue Archéologique de Narbonnaise-Supplément* 44, 293–303.
- Salomon, F., Goiran, J.-P., Pannuzi, S., Djerbi, H., Rosa, C., 2017. Long-term interactions between the Roman City of Ostia and its paleomeander, Tiber Delta, Italy. *Geoarchaeology* 32, 215–229. <https://doi.org/10.1002/gea.21589>.
- Salomon, F., Goiran, J.-P., Noirot, B., Pleuger, E., Bukowiecki, E., Mazzini, I., Carbonel, P., Gadhoun, A., Arnaud, P., Keay, S., Zampini, S., Kay, S., Raddi, M., Ghelli, A., Pellegrino, A., Morelli, C., Germoni, P., 2018. Geoarchaeology of the Roman port-city of Ostia: fluvio-coastal mobility, urban development and resilience. *Earth Sci. Rev.* 177, 265–283. <https://doi.org/10.1016/j.earscirev.2017.10.003>.
- Segre, A.G., 1986. Considerazioni sul Tevere e sull'Aniene nel Quaternario. *Il Tevere e le altre vie d'acqua del Lazio antico*. *Archeologia Laziale* VII, pp. 9–17.
- Shaw, J.B., Ayoub, F., Jones, C.E., Lamb, M.P., Holt, B., Wagner, R.W., Coffey, T.S., Chadwick, J. A., Mohrig, D., 2016. Airborne radar imaging of subaqueous channel evolution in Wax Lake Delta, Louisiana, USA. *Geophys. Res. Lett.* 43, 5035–5042. <https://doi.org/10.1002/2016GL068770>.
- Shepherd, E.J., 2006. Il “Rilievo Topografico di Osita dal Pallone”. *AArea* 115–38.
- Sornoza, L., Barnolas, A., Arasa, A., Maestro, A., Rees, J.G., Hernandez-Molina, F.J., 1998. Architectural stacking patterns of the Ebro delta controlled by Holocene high-frequency eustatic fluctuations, delta-lobe switching and subsidence processes. *Sediment. Geol.* 117, 11–32. [https://doi.org/10.1016/S0037-0738\(97\)00121-8](https://doi.org/10.1016/S0037-0738(97)00121-8).
- Stanley, D.J., Warne, A.G., 1993. Nile Delta: recent geological evolution and human impact. *Science* 260, 628–634.
- Stanley, D.J., Warne, A.G., 1994. Worldwide initiation of Holocene marine deltas by deceleration of sea-level rise. *Science* 265, 228–231. <https://doi.org/10.1126/science.265.5169.228>.
- Stefani, M., Vincenzi, S., 2005. The interplay of eustasy, climate and human activity in the late Quaternary depositional evolution and sedimentary architecture of the Po Delta system. *Mar. Geol.* 222, 19–48.
- Tamura, T., Masuda, F., Sakai, T., Fujiwara, O., 2003. Temporal development of prograding beach–shoreface deposits: the Holocene of Kujukuri coastal plain, eastern Japan. *Mar. Geol.* 198, 191–207. [https://doi.org/10.1016/S0025-3227\(03\)00123-3](https://doi.org/10.1016/S0025-3227(03)00123-3).
- Tanabe, S., Saito, Y., Lan Vu, Q., Hanebuth, T.J.J., Lan Ngo, Q., Kitamura, A., 2006. Holocene evolution of the Song Hong (Red River) delta system, northern Vietnam. *Sediment. Geol.* 187, 29–61. <https://doi.org/10.1016/j.sedgeo.2005.12.004>.
- Ullmann, T., Lange-Athinodorou, E., Göbel, A., Büdel, C., Baumhauer, R., 2018. Preliminary results on the paleo-landscape of Tell Basta/Bubastis (eastern Nile delta): an integrated approach combining GIS-based spatial analysis, geophysical and archaeological investigations. *Quat. Int.* <https://doi.org/10.1016/j.quaint.2017.12.053>.
- Vacchi, M., Marriner, N., Morhange, C., Spada, G., Fontana, A., Rovere, A., 2016. Multiproxy assessment of Holocene relative sea-level changes in the western Mediterranean: sea-level variability and improvements in the definition of the isostatic signal. *Earth Sci. Rev.* 155, 172–197.
- van Asselen, S., Stouthamer, E., van Asch, Th.W.J., 2009. Effects of peat compaction on delta evolution: a review on processes, responses, measuring and modeling. *Earth Sci. Rev.* 92, 35–51. <https://doi.org/10.1016/j.earscirev.2008.11.001>.
- Van Hinte, J.E., 1978. Geohistory analysis—application of micropaleontology in exploration geology. *AAPG Bull.* 62, 201–222.
- Vella, C., Provansal, M., 2000. Relative sea-level rise and neotectonic events during the last 6500 yr on the southern eastern Rhône delta, France. *Mar. Geol.* 170, 27–39. [https://doi.org/10.1016/S0025-3227\(00\)00063-3](https://doi.org/10.1016/S0025-3227(00)00063-3).
- Vella, C., Fleury, T.-J., Raccasi, G., Provansal, M., Sabatier, F., Bourcier, M., 2005. Evolution of the Rhône delta plain in the Holocene. *Marine Geology, Mediterranean Prodelta Systems* 222–223, 235–265. <https://doi.org/10.1016/j.margeo.2005.06.028>.
- Vittori, C., Mazzini, I., Salomon, F., Goiran, J.-P., Pannuzi, S., Rosa, C., Pellegrino, A., 2015. Palaeoenvironmental evolution of the ancient lagoon of Ostia Antica (Tiber delta, Italy). *J. Archaeol. Sci.* 54, 374–384. <https://doi.org/10.1016/j.jas.2014.06.017>.
- Wright, L.D., 1977. Sediment transport and deposition at river mouths: a synthesis. *Geol. Soc. Am. Bull.* 88, 857–868.
- Wright, L.D., 1985. River deltas. In: Jr, R.A.D. (Ed.), *Coastal Sedimentary Environments*. Springer, New York, pp. 1–76. https://doi.org/10.1007/978-1-4612-5078-4_1.
- Wright, L.D., Coleman, J.M., 1973. Variation in morphology of the river deltas as function of ocean wave and river discharge regimes. *Bull. A.A.P.G.* 57, 370–398.
- Yu, S.-Y., Törnqvist, T.E., Hu, P., 2012. Quantifying Holocene lithospheric subsidence rates underneath the Mississippi Delta. *Earth Planet. Sci. Lett.* 331–332, 21–30. <https://doi.org/10.1016/j.epsl.2012.02.021>.
- Zanchetta, G., Drysdale, R.N., Hellstrom, J.C., Fallick, A.E., Isola, I., Gagan, M.K., Pareschi, M. T., 2007. Enhanced rainfall in the Western Mediterranean during deposition of sapropel S1: stalagmite evidence from Corchia cave (Central Italy). *Quat. Sci. Rev.* 26, 279–286. <https://doi.org/10.1016/j.quascirev.2006.12.003>.